An Index to Distinguish Surface- and Subsurface-Intensified Vortices from Surface Observations

C. ASSASSI,[a,b,c] Y. MOREL,[a] F. VANDERMEIRSCH,[b] A. CHAIGNEAU,[a] C. PEGLIASCO,[a] R. MORROW,[a] F. COLAS,[d] S. FLEURY,[a] X. CARTON,[b] P. KLEIN,[b] AND R. CAMBRA[a]

[a] *LEGOS, University of Toulouse, CNES, CNRS, IRD, UPS, Toulouse, France*
[b] *University of Brest, CNRS, IRD, Ifremer, Laboratoire d'Océanographie Physique et Spatiale, IUEM, Brest, France*
[c] *Space Technology Center, Algerian Space Agency, Oran, Algeria*
[d] *LOCEAN (IRD/IPSL/UPMC), Paris, France*

(Manuscript received 6 July 2015, in final form 23 April 2016)

ABSTRACT

In this study, the authors first show that it is difficult to reconstruct the vertical structure of vortices using only surface observations. In particular, they show that the recent surface quasigeostrophy (SQG) and interior and surface quasigeostrophy (ISQG) methods systematically lead to surface-intensified vortices, and those subsurface-intensified vortices are thus not correctly modeled. The authors then investigate the possibility of distinguishing between surface- and subsurface-intensified eddies from surface data only, using the sea surface height and the sea surface temperature available from satellite observations. A simple index, based on the ratio of the sea surface temperature anomaly and the sea level anomaly, is proposed. While the index is expected to give perfect results for isolated vortices, the authors show that in a complex environment, errors can be expected, in particular when strong currents exist in the vicinity of the vortex. The validity of the index is then analyzed using results from a realistic regional circulation model of the Peru–Chile upwelling system, where both surface and subsurface eddies coexist. The authors find that errors are mostly associated with double-core eddies (aligned surface and subsurface cores) and that the index can be useful to determine the nature of mesoscale eddies (surface or subsurface intensified) from surface (satellite) observations. However, the errors reach 24%, and some possible improvements of the index calculations are discussed.

1. Introduction

Superimposed on the large-scale circulation, the ocean is filled with numerous coherent mesoscale eddies whose size typically corresponds to the Rossby radius of deformation between 10 and 300 km (e.g., Chelton et al. 2007, 2011; Morrow and Le Traon 2012). Cyclonic and anticyclonic eddies can advect parcels of trapped fluid over time scales from weeks to months and thus play an important role for the large-scale transfer and redistribution of heat, salt, and momentum (e.g., Wunsch 1999; Jayne and Marotzke 2002; Morrow and Le Traon 2012; Treguier et al. 2012). At local scale, eddies have important implications on tracer dispersion, ocean stirring, and mixing processes (d'Ovidio et al. 2004; Pasquero et al. 2005; Beron-Vera et al. 2008, 2010). Through horizontal and vertical motions, they also affect biogeochemical properties such as nutrients and phytoplankton concentration and can thus impact biological resources and marine ecosystems (McGillicuddy and Robinson 1997; Abraham 1998; Martin and Richards 2001; Lévy and Klein 2004; Pasquero et al. 2005; Bracco et al. 2009). Finally, ocean eddies can also influence the lower-atmosphere winds (Chelton and Xie 2010; Chelton 2013), cloud cover, and rainfall (Frenger et al. 2013) and enhance the dissipation of energy introduced by the wind to the ocean (Munk and Wunsch 1998; Wunsch and Ferrari 2004).

Satellite-based sensing provides sea surface parameters at increasing precision, resolution, and frequencies that are crucial for studying the ocean mesoscale dynamics. Eddies are associated with thermodynamical anomalies with relatively large amplitudes and can have clear signatures on altimetry sea level anomaly (SLA) maps and infrared sea surface temperature (SST) images. Mesoscale vortices can be simply classified into

Corresponding author address: Charefeddine Assassi, Algerian Space Agency (ASAL), Space Technology Center, BP 13 Arzew, 31200 Oran, Algeria.
E-mail: cassassi@cts.asal.dz

DOI: 10.1175/JPO-D-15-0122.1

four distinct categories depending on their rotation sense (cyclonic or anticyclonic) and the vertical position of their potential vorticity (PV) core (surface or subsurface intensified) depending whether their core—or area where their potential vorticity reaches its maximum—is located inside the water column rather than in the surface layer. The rotation sense can be easily retrieved from SLA satellite data considering the geostrophic approximation (Pedlosky 1987; Cushman-Roisin and Beckers 2011). In contrast, surface satellite data do not allow, a priori, determining whether an eddy is surface or subsurface intensified. Using in situ hydrographic data, subsurface eddies have been observed in various sites of the World Ocean, such as the Mediterranean water eddies (meddies) and slope water oceanic eddies (swoddies) in the northeastern Atlantic (Pingree et al. 1992a,b; Paillet et al. 2002; Bashmachnikov et al. 2013), the California Undercurrent eddies (cuddies) in the northeastern Pacific (Garfield et al. 1999), or subsurface anticyclones in the southeastern Pacific (Johnson and McTaggart 2010; Chaigneau et al. 2011; Morales et al. 2012; Stramma et al. 2013). Subsurface-intensified eddies, which are thus ubiquitous in the ocean, are typically centered between 200 and 1000 m depth and exhibit, by nature, a completely distinct vertical structure than surface-intensified vortices (e.g., Chaigneau et al. 2011; Colas et al. 2012).

Different mechanisms of generation can explain the formation of surface or subsurface cyclones and anticyclones. Barotropic and baroclinic instabilities of oceanic currents are known to generate anticyclone and cyclone dipoles (see Cushman-Roisin and Beckers 2011; Morel and McWilliams 2001). They can also be forced by the rough floor topography (Pingree and Le Cann 1992a; Chérubin et al. 2000; Thompson 2008). Many remote sensing observations have also revealed the formation of surface eddies in the lee of islands (Calil et al. 2008). In the latter case, Kubryakov and Stanichny (2015) found a correlation between wind curl and the type of eddy formed; they showed that a weakening of large-scale circulation in response to the decrease of the wind curl leads to the formation of anticyclones and that an increasing wind curl and circulation induce intensive formation of cyclones. A constant wind blowing along a regular coast generates coastal upwelling or downwelling currents that are known to form surface and subsurface eddies (McGillicuddy 2015). Different mechanisms have been proposed to explain the observed instabilities and eddy generation for upwelling systems: adiabatic processes leading to the modification of the potential vorticity structure of the flow and barotropic/baroclinic instabilities, the effect of capes or promontories, or the planetary beta effect when the coast is oriented along a north–south direction (see Marchesiello et al. 2003; Morel et al. 2006; Meunier et al. 2010).

Although both surface- and subsurface-intensified eddies can have a signature on satellite surface data, in particular on SLA and SST anomaly (SSTA) maps, without additional in situ measurements, there exists a strong risk that the surface anomalies associated with subsurface eddies are interpreted as signatures of surface eddies, in particular by data assimilation systems or, as will be shown in this article, by vertical reconstruction methods based on sea surface data, such as the surface quasigeostrophy (SQG; see Blumen 1978; Held et al. 1995; Isern-Fontanet et al. 2006) or the interior and surface quasigeostrophy (ISQG; see Wang et al. 2013) methods. There exist other methods that could potentially be used to reconstruct the vertical structures of subsurface vortices, for instance, the effective surface quasigeostrophic (ESQG) theory proposed by Lapeyre and Klein (2006; see also Ponte and Klein 2013), but they rely on some knowledge or hypothesis of the ocean interior that does not distinguish surface/subsurface vortices. For instance, the ESQG method relies on the calculation of a single mean vertical profile $\alpha(z)$ that depends on interior characteristics (the correlation between the interior potential vorticity anomaly and the stratification). As far as observations are concerned, a few studies have analyzed the surface signature of subsurface vortices observed in situ (see, e.g., Stammer et al. 1991; Sweeney et al. 2003; Caballero et al. 2008), and recently Bashmachnikov et al. (2013) have shown that two meddies, detected at sea, were associated with positive SLA and negative SST anomalies and suggested that this could be used as a proxy to identify meddies. Despite these breakthroughs, we still lack a general theory revealing the exact nature (surface or subsurface) of vortices from satellite surface observations. The main goal of this study is to propose a simple index, combining SLA and SST observations, that allows differentiating between surface- and subsurface-intensified eddies.

The paper is organized as follows. In section 2, we present the quasigeostrophic framework used in our study and the general inversion problem to reconstruct the vortex structure. In section 3, we underline the problematic case of distinguishing and inferring the structure of subsurface vortices. We then define the index that may allow discriminating between surface and subsurface-intensified eddies from surface observations only (section 4). The sensitivity of the index to parameters characterizing the vortex and its environment is discussed in section 5. The validation and efficiency of this index is finally tested in section 6 using a regional model simulation of the southeastern Pacific, where surface and subsurface eddies are found (Chaigneau

et al. 2011; Colas et al. 2012). Concluding remarks are provided in section 7.

2. The model

a. Quasigeostrophic framework

To analyze the physical content of different observed fields, and the possibility to define some combination in order to infer information on the structure of oceanic eddies, it is necessary to define equations linking these physical fields. To deal with mesoscale dynamics and vortices, the simplest equations are the quasigeostrophic ones that express the conservation of the quasigeostrophic potential vorticity (QGPV; see Pedlosky 1987; Cushman-Roisin and Beckers 2011):

$$\mathrm{QGPV} = \Delta\psi + \frac{\partial}{\partial z}\left(\frac{f^2}{N^2}\frac{\partial\psi}{\partial z}\right), \tag{1}$$

where $\Delta = \partial/\partial x^2 + \partial/\partial y^2$ is the horizontal Laplace operator, f is the planetary vorticity or Coriolis parameter (here we consider a constant Coriolis parameter $f = 1 \times 10^{-4}\,\mathrm{s}^{-1}$), ψ is the streamfunction (proportional to the pressure field $P = \rho_0 f\psi$), and N is the Brunt–Väisälä frequency, given by

$$N^2 = \frac{-g\partial_z\overline{\rho}}{\rho_0}, \tag{2}$$

where g is the gravitational acceleration and $\overline{\rho}(z)$ is the mean density profile, depending only on the vertical coordinate z and coming from the total stratification expressed as

$$\rho_{\mathrm{tot}} = \rho_0 + \overline{\rho}(z) + \rho, \tag{3}$$

where ρ_0 is a constant reference density and ρ is the departure from this reference profile and is given by (hydrostatic approximation)

$$\rho = -\frac{1}{g}\frac{\partial P}{\partial z} = -\frac{f\rho_0}{g}\frac{\partial\psi}{\partial z}. \tag{4}$$

In the following, we will also consider the sea surface elevation η, or SLA, and the relative vorticity ζ (used to evaluate the strength of a vortex):

$$\eta = \frac{P(z=0)}{\rho_0 g} = \frac{f}{g}\psi, \quad \text{and} \tag{5}$$

$$\zeta = \frac{\partial V}{\partial x} - \frac{\partial U}{\partial y} = \nabla^2\psi. \tag{6}$$

Using the previous relationships, the knowledge of potential vorticity allows for the calculation of all physical fields (see Blumen 1978; Bishop and Thorpe 1994), but the boundary conditions are strong constraints for this inversion, as Eq. (1) is elliptic. Both lateral and vertical boundary conditions thus have to be specified to close this so-called Dirichlet–Laplace problem and to allow the calculation of the streamfunction and all fields from the knowledge of the QGPV. At the vertical boundaries, the condition is generally to specify the density anomaly, which leads to

$$\left.\frac{\partial\psi}{\partial z}\right|_{z=0} = -\frac{g}{\rho_0 f}\rho(z=0), \quad \text{and} \tag{7}$$

$$\left.\frac{\partial\psi}{\partial z}\right|_{z=-H} = -\frac{g}{\rho_0 f}\rho(z=-H), \tag{8}$$

where H is the depth of the ocean. As far as horizontal boundaries are concerned, in the following, in order to invert potential vorticity and calculate the associated velocity, vorticity, or stratification, we have assumed periodic horizontal boundary conditions (see Isern-Fontanet et al. 2006; Wang et al. 2013). Using Fourier transforms, the QGPV inversion then boils down to a 1D (vertical) partial differential equation and can be more easily solved using the vertical barotropic and baroclinic modes associated with the stratification (see Wang et al. 2013).

b. General configuration

We will consider vortices associated with localized QGPV and surface density anomalies. A first important theoretical constraint exists on QGPV and surface/bottom density anomalies. Indeed, integrating vertically Eq. (1) yields [using Eqs. (7), (8), and (2)]

$$\Delta\overline{\psi} = \overline{\mathrm{QGPV}} - \frac{1}{H}\left[\frac{f\rho(z=0)}{\frac{\partial\rho}{\partial z}(z=0)} - \frac{f\rho(z=-H)}{\frac{\partial\rho}{\partial z}(z=-H)}\right], \tag{9}$$

where $\overline{\psi}$ and $\overline{\mathrm{QGPV}}$ are the barotropic (vertical average) streamfunction and QGPV. As shown in Morel and McWilliams (1997), the vortex is "isolated" if the net horizontal integral of the right-hand side (potential vorticity and vertical boundary density anomalies) vanishes. If this is not the case, the vortex is not isolated and its velocity field decreases as $1/r$ (where r is the distance from its center). Such a slow decrease is not realistic (see Zhang et al. 2013) and causes some problems for the inversion in a finite domain. Also, notice that its kinetic energy would be infinite in an unbounded domain and its sea level anomaly would increase as $\log r$.

To avoid this and to deal with isolated and stable vortices, we have chosen to determine a family of vortex structures satisfying the isolation constraint. The QGPV

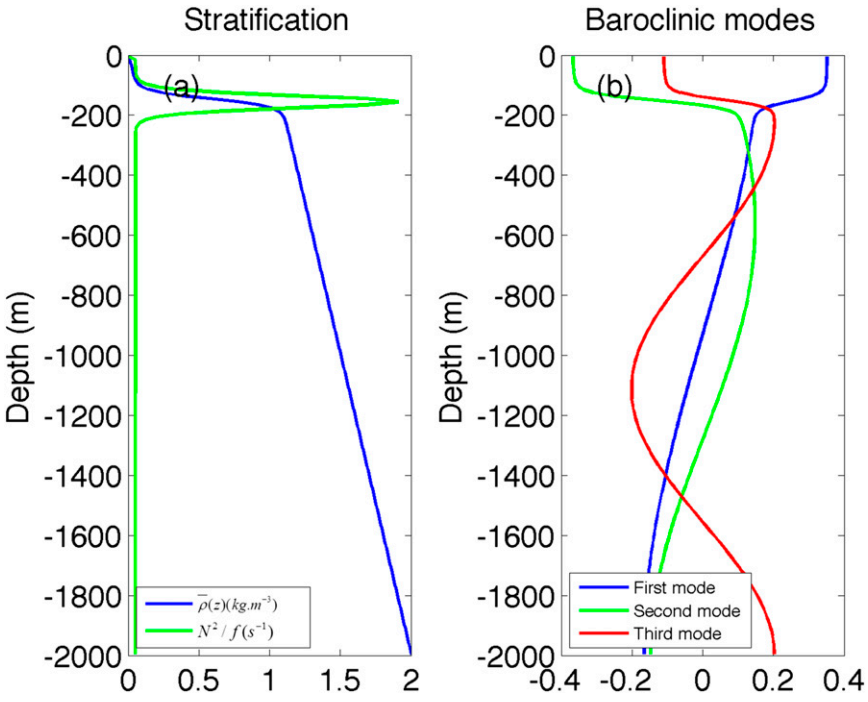

FIG. 1. (a) Chosen density profile $\overline{\rho}(z)$ (blue) and stratification (green) and (b) vertical structure of the first three baroclinic modes.

and surface density anomalies are thus chosen as follows (see Carton and McWilliams 1989; Herbette et al. 2003):

$$\mathrm{QGPV} = Q_0[1-(r/R)^2]e^{-(r/R)^2}e^{-[(z-z_0)/H_v]^2}, \quad (10)$$

$$\rho(z=0) = \delta\rho_0[1-(r/R)^2]e^{-(r/R)^2}, \quad (11)$$

where r is the distance from the vortex center, R is the vortex radius, z is the vertical coordinate (directed upward with $z = 0$ at the surface, so that $z < 0$ within the water column), z_0 is the vertical position of the vortex core, and H_v is its vertical extension. In the following, we consider $R = 50\,\mathrm{km}$, $H_v = 200\,\mathrm{m}$, and the density anomaly at the bottom is considered null, but Q_0, z_0, and $\delta\rho_0$ remain variable.

Notice the structures given by Eqs. (10) and (11) ensure that Eq. (9) is verified, and the vortex is thus isolated. As a result, the knowledge of the streamfunction at lateral boundaries becomes trivial to invert Eq. (1); periodic boundary conditions and fast Fourier transforms can thus be used. Notice in particular that the potential vorticity structure given by Eq. (10) ensures a vanishing net QGPV and is constituted of a core surrounded by a crown of opposite-sign anomaly. Other choices are possible, in particular, the vertical superimposition of opposite-sign PV cores. The latter structure is, however, baroclinically unstable (see Morel and McWilliams 1997), whereas the chosen family of QGPV structures is generally stable (see Carton and McWilliams 1989; Herbette et al. 2003).

Finally, Eqs. (1), (7), and (8) are solved using horizontal and vertical discretizations of $\Delta x = 5\,\mathrm{km}$ and $\Delta z = 10\,\mathrm{m}$. The domain will thus be constituted of a square (biperiodic in the horizontal) basin of length 500 km and total depth $H = 2000\,\mathrm{m}$. The background stratification $\overline{\rho}(z)$ and N^2/f are also fixed and given in Fig. 1a. It represents a seasonal thermocline located between 100 and 200m with a density jump $\delta\rho = 1‰$, which separates two weakly stratified surface and bottom layers. Figure 1b represents the first, second, and third baroclinic modes associated with this stratification. The first radius of deformation is $R_1 = 16\,\mathrm{km}$.

3. The difficult case of subsurface-intensified vortices

As surface fields are accessible from spatial observations, and interior fields are more difficult to obtain at high resolution, it is tempting to try to reconstruct the vertical structure of eddies from the knowledge of surface fields alone. However, if the Dirichlet–Laplace problem, determined by Eqs. (1), (7), and (8) and additional lateral boundary conditions, is a well-posed

mathematical problem, the determination of the streamfunction (and all other physical 3D fields) from the knowledge of surface boundary fields alone is unfortunately ill posed. Indeed, notice that given a surface density field, an infinite number of solutions exist with drastically different 3D fields, provided different interior QGPV fields are chosen. The knowledge of, or some hypothesis on, the interior QGPV field is required to determine the 3D structure of a vortex.

The SQG approach (see Hoskins et al. 1985; Held et al. 1995; Isern-Fontanet et al. 2006), is based on the assumption of no potential vorticity anomaly inside the water column (QGPV = 0), so that the dynamics is entirely determined by the knowledge of the sea surface density anomalies. As noted by Lapeyre and Klein (2006), this hypothesis is generally not well verified, and interior PV has to be taken into account too. Indeed, as shown in appendix A, the vortex structure reconstructed by the SQG method is systematically surface intensified, and it is not possible to reconstruct subsurface vortices.

Recently, Wang et al. (2013) proposed using the knowledge of both the surface density and SLA to determine the 3D structure of a vortex. This overdetermination of the surface boundary condition can indeed lead to some information on the interior QGPV structure and improve the calculation of the 3D structure. Their method, the ISQG method, relies on the combination of the SQG streamfunction ψ_{SQG} (associated with the surface density anomaly alone) and an interior streamfunction ψ_i (associated with the QGPV; see also Lapeyre and Klein 2006):

$$\psi = \psi_{\mathrm{SQG}}(x, y, z) + \psi_i(x, y, z). \tag{12}$$

At the surface, $\psi(x, y, z = 0) = \mathrm{SLA} = \psi_{\mathrm{SQG}}(x, y, 0) + \psi_i(x, y, 0)$. Thus, the difference between the observed SLA and the surface SQG streamfunction (calculated using the observed surface density only) is the signature of the interior QGPV. This proves that the surface boundary overdetermination indeed allows inferring some information of the 3D structure.

Despite this promising result, the interior structure is only known at the surface, and its vertical variation remains unknown. To close the problem, some additional information has to be specified, and Wang et al. (2013) hypothesize that the vertical structure of the interior streamfunction (and QGPV) projects on the barotropic and first baroclinic mode only. Unfortunately, the latter hypothesis leads to the same problem as the SQG method, and the vortex structure reconstructed by the ISQG is systematically surface intensified and is not able to identify subsurface vortices (see appendix A).

The ESQG theory, proposed by Lapeyre and Klein (2006) and extended by Ponte and Klein (2013), can potentially associate sea surface height (SSH) with subsurface structures, but it relies on the knowledge of the interior ocean characteristics and is thus not considered here.

To conclude, the reconstruction of the 3D structure of vortices from the knowledge of surface fields alone is ill posed and relies on additional hypothesis that, to our knowledge and up to now, systematically leads to surface-intensified structures. The improvement of the existing methods requires being able to reconstruct the structures of both surface- and subsurface-intensified vortices. An indication to determine if the observed surface anomalies are associated with a surface- or a subsurface-intensified structure would thus be an important step for such an improvement.

4. Definition of an index to identify surface- and subsurface-intensified eddies

If the complete 3D structure of a vortex seems difficult to calculate precisely from surface fields alone, its nature, surface or subsurface, is simpler to determine. Indeed, for instance, anticyclonic vortices are always associated with a positive SLA, but the sea surface density anomaly depends on the vertical position of the vortex core: it is expected to be negative for surface-intensified anticyclones (see Fig. 2a) but positive when the vortex core is subsurface, as shown by Bashmachnikov et al. (2013) for meddies. Thus, the combination of SLA and sea surface density anomaly can lead to the identification of the vortex nature.

The shape of isopycnal levels for subsurface- and surface-intensified eddies is illustrated in Fig. 2a. Surface-intensified cyclones are associated with a negative SLA and outcropping of isopycnals, leading to positive sea surface density (SSρ) anomalies. In contrast, surface-intensified anticyclones are associated with a positive SLA and deepening of isopycnals, leading to a negative SSρ. Thus, the ratio SSρ/SLA is expected to be negative for both surface-intensified cyclones and anticyclones. Subsurface-intensified anticyclones still have positive SLA; however, the typical shape of isopycnal levels is lens-like, with isopycnic levels outcropping the surface (McWilliams 1985; Stammer et al. 1991; McGillicuddy et al. 1999; Sweeney et al. 2003; Sánchez and Gil 2004). This results in opposite sign of SSρ anomalies in comparison with surface-intensified vortices, and the ratio SSρ/SLA is thus positive for both anticyclonic and cyclonic subsurface vortices.

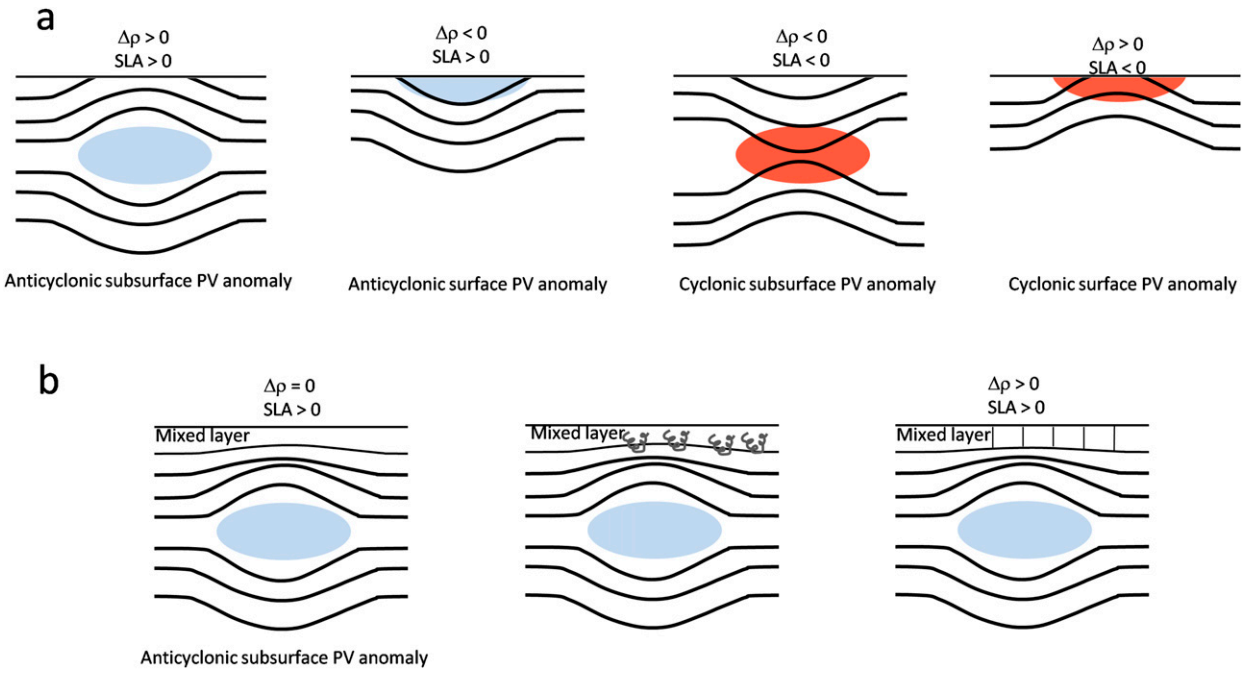

FIG. 2. Isopycnal displacements, SLA, and SST anomaly for (a) the four different eddy types and (b) a subsurface eddy with a mixed layer.

We thus define

$$\chi_\rho = \frac{\mathrm{SS}\rho}{\mathrm{SLA}}, \tag{13}$$

whose sign can be used to discriminate between surface and subsurface-intensified eddies. The use of χ_ρ could be problematic when there exists a homogeneous mixed layer topping a subsurface vortex (surface vortices are always characterized by density anomalies). However, as shown in Fig. 2b, we expect the signature to be the same for χ_ρ. Indeed, for an anticyclone, the thermocline will be deformed similarly to the isopycnic levels below. In addition, the density anomaly just below the thermocline is also higher above the vortex. When mixing occurs, both previous effects contribute to the creation of positive SSρ anomalies above the vortex core (see Fig. 2b), leading to a positive χ_ρ.

Finally, as SSρ is not directly measured from satellite observations, we also define

$$\chi_T = \frac{\mathrm{SST}}{\mathrm{SLA}}. \tag{14}$$

At first order, the variations of SSρ are dominated by SST variations (except in specific regions where salinity can play a substantial role on the stratification: near estuaries, region of ice formation/melting, etc.), and SST can be observed remotely. Thus, χ_T can also be used as an index to distinguish between surface- and subsurface-intensified eddies (this will be tested and confirmed in section 6e), except that as temperature and density are anticorrelated, χ_ρ and χ_T are of opposite sign (see Table 1).

5. Sensitivity and errors estimation

Qualitative arguments show that the sign of χ_ρ can determine the nature of a vortex in simple configurations, with monopolar, circular, and isolated vortices (here meaning that there is no background flow). The latter simplifications are generally not verified in nature, and the consequence on the validity of our criterion has to be evaluated.

We believe that the deformation of vortices (elliptic shapes or inclination of the vertical axis) is not problematic: tests have shown that, as long as the vortex remains coherent (horizontal deformation below two

TABLE 1. Sign of indices and SLA for the different vortex types.

χ_ρ = SSρ/SLA	χ_T = SST/SLA	SLA	Nature of the vortex
>0	<0	>0	Subsurface and anticyclonic
>0	<0	<0	Subsurface and cyclonic
<0	>0	>0	Surface and anticyclonic
<0	>0	<0	Surface and cyclonic

initial vortex radius), the nature of deformed vortices remain correctly detected by the index.

When a background flow exists, the first problem is to identify and calculate the part of the SSρ and SLA signal associated with the vortex and the background flow. A filter has to be designed, and we have proposed to use a spatial average based on a Gaussian filter with a correlation radius R_f (see appendix B). This filter is used to calculate and remove the background flow but is obviously a source of error: it alters the vortex structure, and the separation between vortex structures and background flow is not obvious if their scales are comparable. To evaluate possible errors, we propose to consider vortices for which the streamfunction can be described by a Gaussian structure in the horizontal (Chelton et al. 2011), and we also assume a localized (again Gaussian) vertical extension:

$$\psi = \psi_{0v} e^{-(r/R)^2} e^{-[(z-z_0)/H_v]^2}, \tag{15}$$

where ψ_{0v} is the streamfunction maximum, R is the vortex radius, z_0 is the vertical position of the vortex core, and H_v is its vertical extent. Notice that, for the sake of simplicity, the vortex streamfunction structure is here expressed directly. We could have used Eqs. (10) and (11), but the problem would have been more complicated as the background stratification would have played a role. Our goal is simply to qualitatively illustrate the possible problems associated with the index calculation, so we chose a less realistic but simpler way of specifying the vortex. Note that the vortex is still subsurface for $z_0 < 0$. We then superimpose a jetlike surface current with a streamfunction of the form:

$$\psi = \psi_{0j} \tanh\left(\frac{y - y_0}{L}\right) e^{-z/H_j}, \tag{16}$$

where L is the width of the current, H_j is its vertical extension, and y_0 is the distance between the current and the vortex center. In the following, we consider, $H_j = 200\,\text{m}$, but ψ_{0j}, y_0, and L remain variable. We also consider a subsurface anticyclonic vortex, with fixed characteristics [Gaussian structure defined using Eq. (15)]: intensity $\psi_{0v} = 7500\,\text{m}^2\,\text{s}^{-1}$, vertical position $z_0 = -200\,\text{m}$, vertical extent $H_v = 400\,\text{m}$, and radius $R = 50\,\text{km}$. We superimpose both flows and use the filter given in appendix B to isolate the vortex flow and calculate χ_ρ. The vortex is subsurface, so that we expect $\chi_\rho > 0$.

We evaluated the sensitivity of the index calculation to the filter correlation radius R_f and jet width L, the jet intensity and its width, and the jet intensity and the position of the jet with respect to the eddy center y_0. The results are shown in Fig. 3. Figure 3a represents the

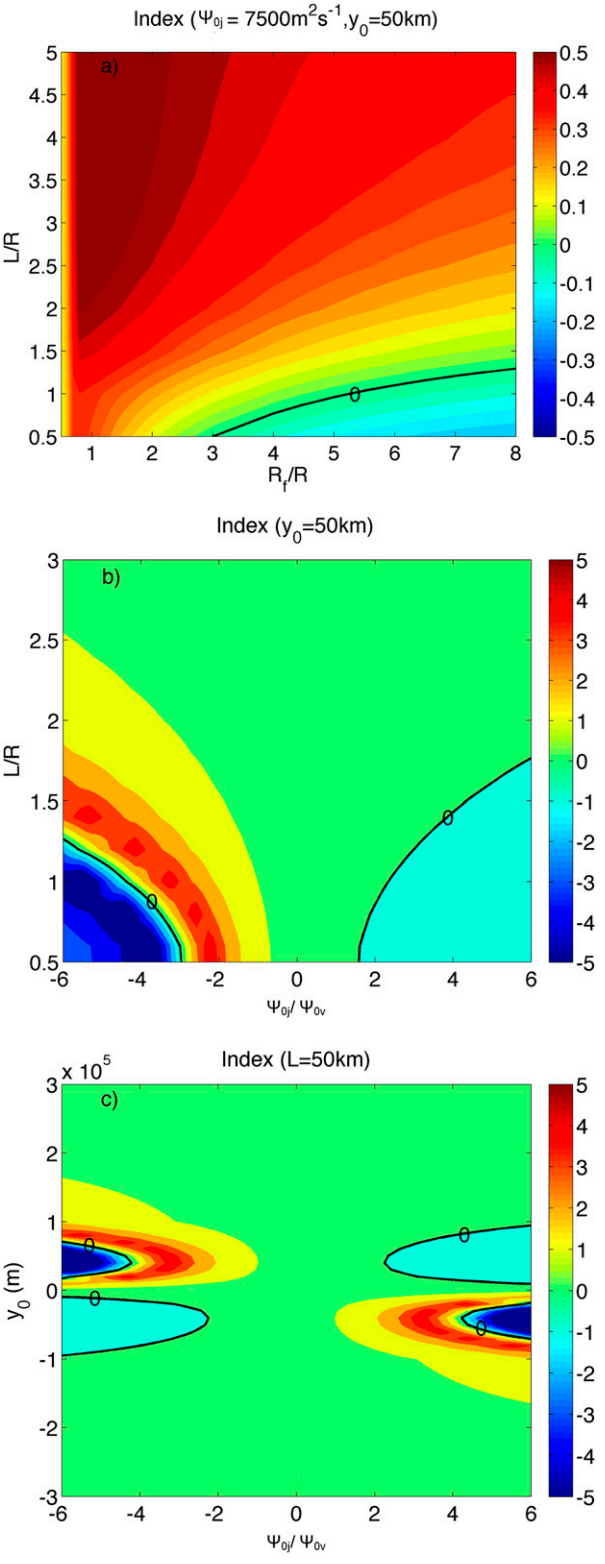

FIG. 3. Sensitivity study of the index to (a) the filter radius and the current width, (b) the jet intensity and its width, and (c) the jet intensity and the distance between jet and eddy.

index values as a function of the filter correlation radius and jet width. We have chosen $\psi_{0j} = \psi_{0v} = 7500\,\mathrm{m^2\,s^{-1}}$ and $y_0 = 50\,\mathrm{km}$ (this corresponds to the most unfavorable distance, as can been seen in Fig. 3c). The $\chi_\rho = 0$ isoline is represented so that it is easy to determine filter and jet characteristics for which the index calculation is problematic, here associated with a negative index that would identify the vortex as surface intensified. When R_f is small, the filter is not active and both structures (jet and vortex SLA and SSρ signatures) mix so that the evaluation of the vortex nature is problematic, whatever the value of the jet width. A minimum filter correlation radius is thus necessary to avoid this problem. Also, as can be seen from Fig. 3a, wrong identification is possible when the filter radius is more than 3 times the eddy radius and current width, being comparable to or less than about 1.3 eddy radii. Otherwise, the eddy is always correctly identified as subsurface. This shows that the correlation radius of the Gaussian filter has to be chosen so that $R_f < 3R$. In addition, we can observe that, when the current width and the vortex have the same size ($L/R = 1$), the best results are obtained when $R_f \sim R$.

Figure 3b represents the index values as a function of the jet width and jet intensity. We thus set the filter radius to 50 km and the distance eddy jet y_0 to +50 km. As can be expected, background currents influence the calculation of the index and can lead to incorrect identification if their characteristics (width and intensity) become comparable to the eddy. Also notice that there is no symmetry between eastward ($\psi_{0j}/\psi_{0v} > 0$) and westward current ($\psi_{0j}/\psi_{0v} < 0$); this is related to the clockwise rotation of the anticyclonic eddy that has accumulative effect on the eastward current and opposite effects when the current is westward. To conclude, close to strong and narrow currents, the detection of the nature of eddies can be problematic.

Figure 3c represents the index variations as a function of the jet intensity and vortex–current distance. Here we have chosen $R_f = 50\,\mathrm{km}$ and $L = 50\,\mathrm{km}$. Again, there is no detection problem when the current is weak enough or when the current is far from the vortex. Notice that, when the center of the eddy is exactly superimposed with the current ($y_0 = 0$), the subsurface eddy is well detected too, because in this particular point the average of the sea surface height and of the density fields associated with the current are weak. However, for strong currents (intensity higher than 2.3 times the vortex intensity), and when the vortex strongly interacts with the current ($y_0 \sim R$), the index does not allow a correct detection of the vortex nature.

To conclude, we have here illustrated that, in a complex environment, when the vortex is in the vicinity of strong currents, the χ_ρ index can lead to incorrect identification of the nature (surface or subsurface) of a vortex.

6. Validation of χ_ρ and χ_T using a realistic numerical simulation

a. Model configuration

To examine the general relevance of the proposed indices (χ_ρ and χ_T), we now use a realistic simulation of the Peru–Chile Current System. In this region, the main characteristics and dynamics of mesoscale eddies have been recently studied from satellite data and in situ observations (Chaigneau and Pizarro 2005a,b; Chaigneau et al. 2008, 2009, 2011; Johnson and McTaggart 2010; Morales et al. 2012; Stramma et al. 2013). These studies have revealed the presence of both surface- and subsurface-intensified eddies that are preferentially formed near the coast and propagate toward the open ocean. The Regional Ocean Modeling System (ROMS) is used to reproduce the observed regional circulation (Penven et al. 2005; Colas et al. 2008; Montes et al. 2010, 2011; Echevin et al. 2011) where both surface and subsurface eddies exist (Colas et al. 2012).

ROMS is a free-surface, split-explicit model that solves the hydrostatic primitive equations based on the Boussinesq approximation (Shchepetkin and McWilliams 2005; 2009). We used the configuration developed in Colas et al. (2012, 2013). The horizontal grid is isotropic and spans the region between 15°N and 41°S and from 100°W to the South American coast. The baroclinic Rossby radius of deformation is 50–150 km in the region (e.g., Chelton et al. 1998; Chaigneau et al. 2009) and the spatial resolution is ~7.5 km, allowing us to resolve mesoscale structures (Colas et al. 2012). Thirty-two stretched terrain-following curvilinear vertical coordinates are used. Lateral boundaries are opened and forced by thermodynamical fields from the Simple Ocean Data Assimilation (SODA) monthly climatology (Carton and Giese 2008), constructed over the 1980–2000 period. The model is forced at the surface by heat fluxes from the COADS monthly climatology (DaSilva et al. 1994) and by a QuikSCAT monthly climatology for the wind stress (SCOW; Risien and Chelton 2008). As in Colas et al. (2012), the simulation was performed over a 13-yr period, and outputs are 3-day average fields. The first 3 years are considered as the spinup phase and discarded from the stabilized equilibrium solution analyzed in this study. The mean currents are realistic and major characteristics of the Humboldt Current system are reproduced, but El Niño events and intraseasonal variability associated with equatorial waves dynamics are not represented because of the climatological forcing. In the present study, we first use the last year of the simulation for our analysis.

Figure 4 represents the sea surface height and temperature for a given model output (1 February of the fourth year of the simulation, that is to say, 1 month after the spinup phase), representative of the circulation in the area. Notice the presence of numerous eddies, but also the larger-scale gradients associated with the large-scale circulation and the strong coastal upwelling associated with permanent alongshore winds (Colas et al. 2012). Since alongshore equatorward wind is the primary forcing of coastal upwelling along an eastern boundary, this upwelling is ubiquitous, as indicated by the continuous strip of cold water and negative SSH near shore (Fig. 4). Interested readers are referred to Colas et al. (2012, 2013) for a more detailed analysis of the simulation.

b. *Analysis of surface and subsurface eddies*

The determination of the vortex nature from surface fields is done in five steps:

1) Extract snapshots of the SSH and SSρ (or SST) fields from the simulation.
2) Apply a spatial filter to the latter fields to calculate "anomalies": SLA, SSρA, and SSTA. The horizontal averaging given in appendix A is used to calculate mean fields and the anomalies are the difference between the initial fields and the mean fields.
3) Calculate χ_ρ = SSρA/SLA (or χ_T = SSTA/SLA). To avoid problems where SLA = 0, we calculate χ_ρ = (SSρA × SLA)/max(SLA^2, ε), where $\varepsilon = 10^{-4}$ cm^2.
4) Identify all vortices: we identify all local SLA extrema for which |SLA| ≥ 2 cm. The extrema are associated with the vortex centers.
5) Determine the expected nature of each vortex: we calculate the average value of the index near each vortex center (average over 1 grid point). The vortex is identified as subsurface intensified if $\chi_\rho > 0$ and surface intensified if $\chi_\rho < 0$.

Concerning the filtering step, we use a Gaussian filter (see appendix B), and as described above, the correlation radius R_f of the filter should be chosen close to the vortex radius and smaller than 3 times the latter. As in this region the eddy size ranges between 50 and about 150 km (Chaigneau et al. 2008, 2009); we have thus chosen R_f = 150 km.

The anomaly maps (SLA, SSρA, and SSTA) corresponding to Fig. 4 are shown in Fig. 5. The SLA exhibits positive changes up to 8 cm for anticyclonic eddies and −10 cm for cyclonic eddies. The structure of the vortices is well marked (Fig. 5a). The SSρA and SSTA exhibit very similar structures, with SSTA variations reaching ±1°C in the open ocean but as low as −4°C near the coast where the upwelling signal is very strong.

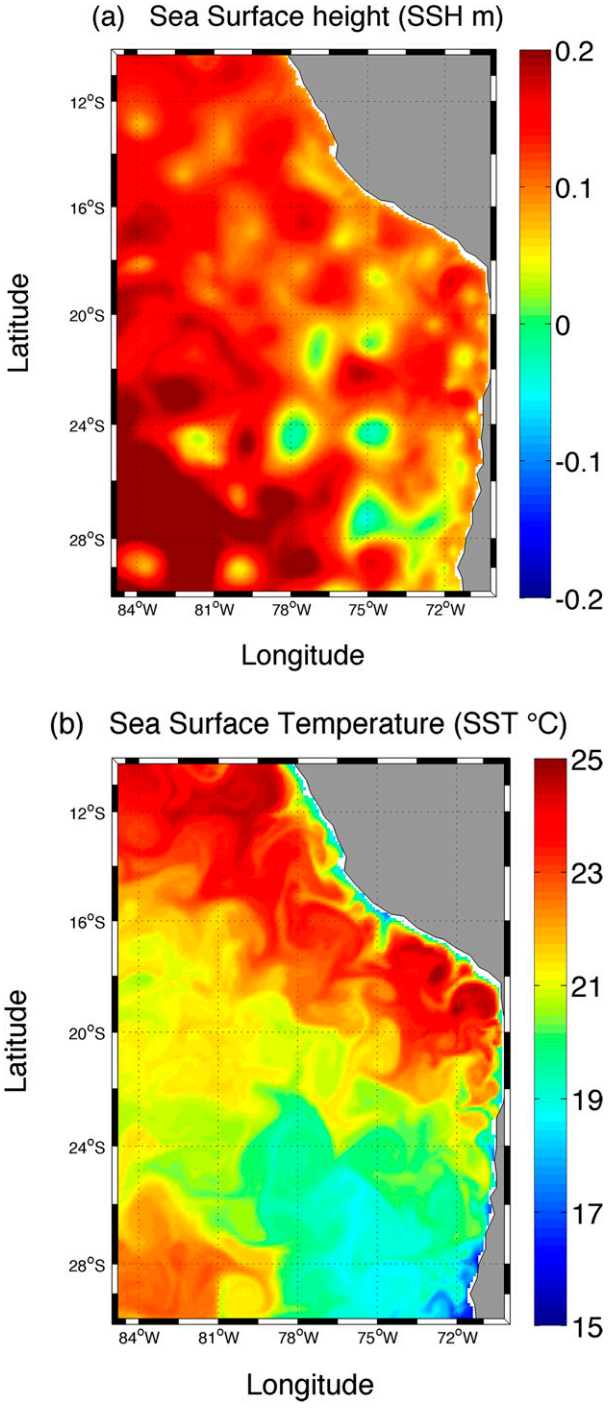

FIG. 4. (a) SSH (m) and (b) SST (°C) over the Peru–Chile domain on 1 February of the last (seventh) year of the climatological simulation.

The vortex structures are more clearly marked on SLA than on SSρA or SSTA maps (see Figs. 5b,c). Vortex centers are thus identified as local extrema on SLA maps. To avoid taking into account relatively weak eddies, we discarded eddies having a |SLA| < 2 cm.

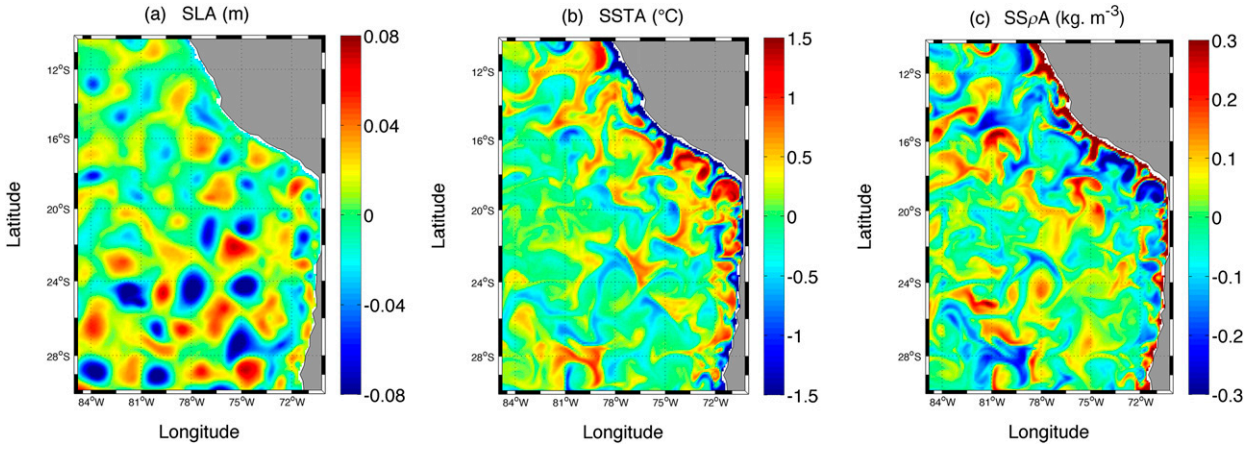

FIG. 5. (a) SLA (m), (b) SSTA (°C), and (c) SSρA (kg m^{-3}), where the anomalies are calculated from the total fields presented in Fig. 4.

Figure 6 shows a map of SSρA, on which we have superimposed SLA contours. Note that both fields, which enter in the calculation of χ_ρ, generally exhibit coherent patterns. However, SSρA exhibits a more complex structure, with marked filaments sometimes penetrating vortex cores.

Figure 7 shows a map of χ_ρ, where red areas are associated with positive values, corresponding to expected subsurface vortices, and blue areas are associated with negative values, corresponding to expected surface vortices. We have also superimposed the filtered SLA isolines (yellow contours).

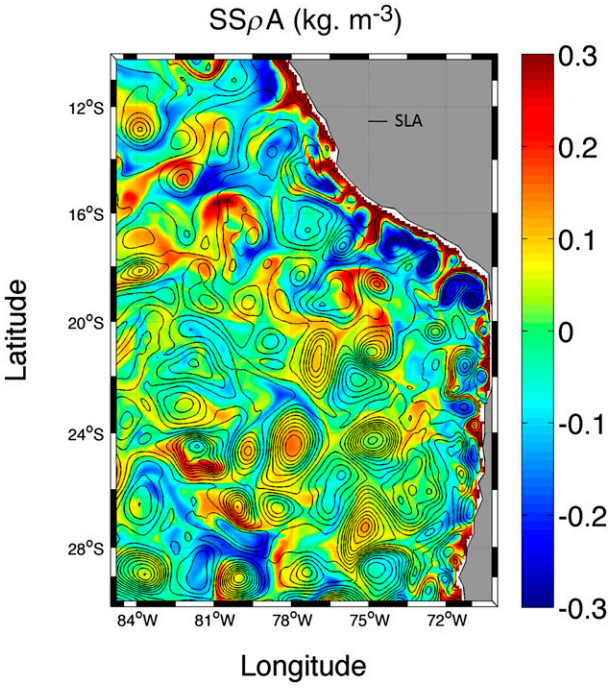

FIG. 6. SSρA (kg m^{-3}; color) with SLA (black lines) superimposed.

The expected nature of the vortex, calculated using the index, is then compared to the exact nature of the identified vortex that is established using the relative vorticity (calculated from the total 3D velocity field available from the numerical results). Based on the

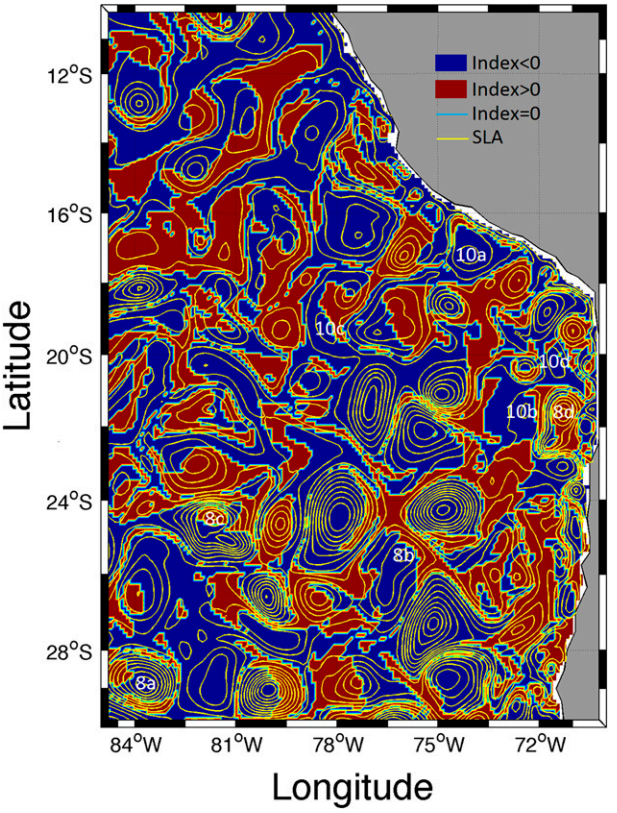

FIG. 7. Map of the index χ_ρ (red for positive index and subsurface vortices, blue for negative index and surface vortices) with SLA (yellow lines) superimposed in the Peru–Chile area calculated from the fields presented in Fig. 5 (the positions of specific eddies analyzed in this study are indicated by numbers).

notion that rotation dominates within a vortex, the relative vorticity is indeed a good indicator and can be used to detect eddies and to characterize their intensity (McWilliams 1990). For each detected vortex, the depth of maximum absolute relative vorticity $|Z_{\zeta\max}|$ corresponds to the vertical position of the vortex core. Vortices will be considered surface intensified when $|Z_{\zeta\max}|$ is located within the mixed layer (whose thickness is about 30–50 m for the present simulation), and subsurface when it is located below.

The four different vortex types were observed: surface anticyclones and cyclones (with respective positive and negative relative vorticity reaching their maximum absolute value at the surface) and subsurface anticyclones and cyclones (with respective positive and negative relative vorticity reaching their maximum absolute value inside the water column). Typical examples are given in Fig. 8 with structures representative of the four possible vortex types and different amplitudes. The positions of the chosen eddies are indicated on Fig. 7 (denoted 8a–d).

c. *Analysis*

For the particular SLA map shown in Fig. 5a, 77 eddies have been identified over the region. Figure 9 represents the position for all identified eddies superimposed on the SLA (Fig. 9a) and χ_ρ (Fig. 9b). Crosses (+) represent eddies that are correctly identified by χ_ρ; stars (*) represent eddies that are not correctly identified by χ_ρ: positive index but surface-intensified core in reality or negative index but subsurface-intensified core. Among the 77 eddies detected, 24 (30%) are not correctly identified. As we will see below, this error rate corresponds to a maximum in the simulation (summer season).

There exist two main types of vortices leading to incorrect identification: eddies with a clear main core and a well-defined structure and eddies having a multicore structure with superimposed surface and subsurface maxima of relative vorticity.

Figure 10 represents the relative vorticity structure of four eddies for which the index yields wrong results. Their positions are indicated in Fig. 7 (denoted 10a–d) and Fig. 9 (indicated by stars). Vortex 10a is a subsurface anticyclonic vortex identified as a surface-intensified eddy by the index χ_ρ (negative value). Vortex 10b is a surface-intensified anticyclone identified as a subsurface-intensified eddy by the index. Notice that most of these vortices have an index that varies from negative to positive in the vicinity of the center (see Figs. 9 and 6). Vortices 10c and 10d are different and are associated with a multicore structure (Figs. 10c,d, vertical transects). The strength of both cores is similar so that is difficult to identify the main core.

Multicore structures represent a bit more than half the problematic cases. It does not seem possible to identify multicore vortices without complementary vertical profiles. In practice, any method based on surface observations can thus only reconstruct half the structure (the surface or the subsurface part). Multicore eddies represent a significant fraction in the present simulation, but many of them can be considered as eddies with a main core (one of the cores is much stronger than the others) and do not cause particular problems. Multicore structures with cores of similar strength are more problematic. Even though they are rarely observed in nature (see Pingree and Le Cann 1993; Tychensky and Carton 1998), it is well known that vortices of the same sign but whose cores are located at different depths tend to align when they are close to each other (Polvani 1991; Nof and Dewar 1994; Correard and Carton 1998; Sutyrin et al. 1998; Perrot et al. 2010). It has also been shown that the interaction of vortices with currents or topography can lead to the formation of secondary aligned poles for the vortex (Vandermeirsch et al. 2002; Herbette et al. 2003, 2004). The present results show that they could be more frequent than expected, at least in numerical simulations, but their identification requires in situ observations.

To conclude, the use of the index χ_ρ allows us to adequately determine the nature of the eddy (surface or subsurface) for about 70% of them in this specific output, and among the incorrect detections about half are associated with vortices that are both surface and subsurface.

d. *Statistics over seven years*

To evaluate whether the previous results depend on the specific date chosen above, in particular on seasonal characteristics of the mixed layer (depth, enhanced winter mixing, or summer restratification), the previous calculations have been tested for other dates over the 7 years of simulation. Output corresponding to the first of each month have been selected and analyzed. More frequent outputs can be used, but since the vortex evolution is on the order of a few weeks, one month is an adequate time period to have considerable evolution of the vortex distribution but still have a good representation of the seasonal variability. For each selected date, we follow the methods presented in the previous section: all vortices have been identified, the index χ_ρ and the vortex core depth $Z_{\zeta\max}$ have been calculated and visually compared with the vertical relative vorticity structure, and multicore structures have been identified.

The global statistics are presented in Fig. 11, which represents the total number of vortices detected and the number of wrong identification for the 12 months of the simulation (mean of 7 years and the standard deviation).

This graphic shows that the total error varies between 15% and 30% and represents an average of 24%, so that 76% of the vortices are correctly identified.

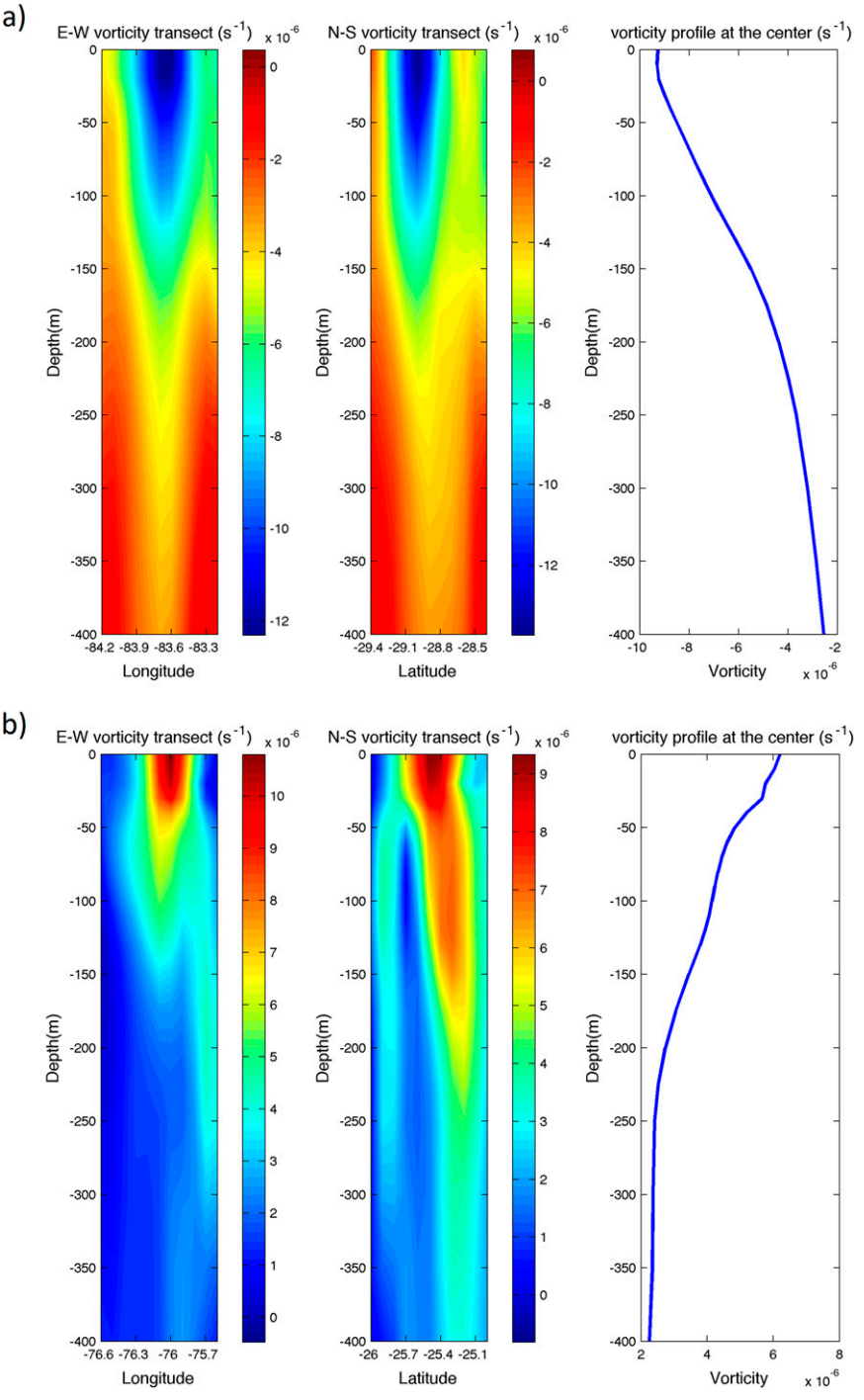

FIG. 8. Relative vorticity (east–west and north–south transects, vertical profile) of eddies correctly identified: (a) cyclonic surface eddy, (b) anticyclonic surface eddy, (c) cyclonic subsurface eddy, and (d) anticyclonic subsurface eddy. The position of each vortex (denoted 8a–d) is indicated in Fig. 7.

Multicore eddies represent 58% of the wrong identification (explaining 14% of the 24% errors). The error, associated with eddies having a main core, has an average of ~10%, which is considered good. Interestingly, this error exhibits a seasonal cycle with a minimum in austral winter and a maximum in late austral summer. This is associated with mixed layer dynamics. Indeed, during summer, when the mixed layer is shallower, SSTA can be more influenced

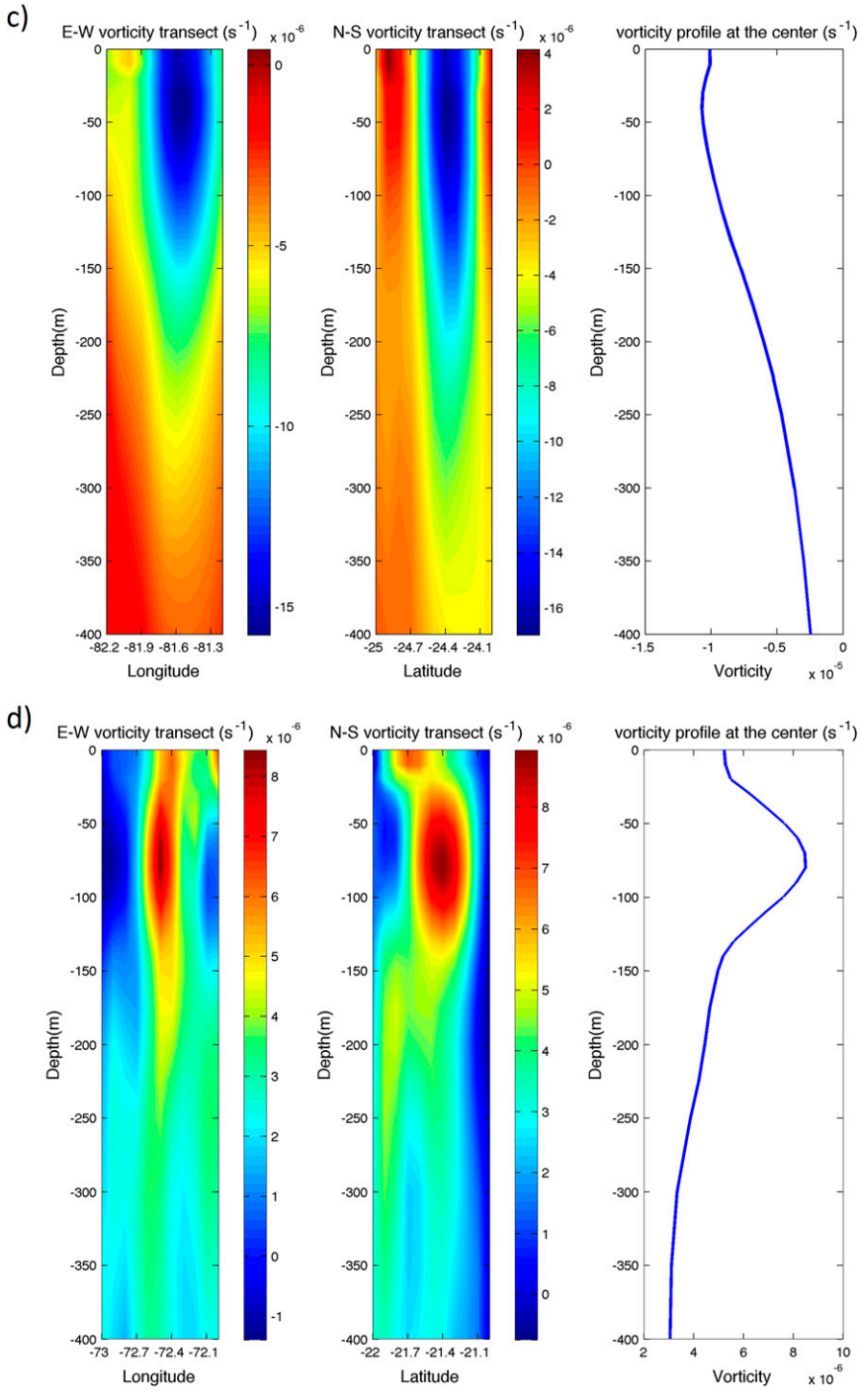

FIG. 8. (*Continued*)

by atmospheric forcings than by oceanic processes. In addition, during summer, the stratification increases and the mixed layer shrinks, reducing the surface signature of subsurface-intensified eddies.

To conclude, despite the observed seasonal variability, the errors remain reasonable and the index is able to correctly identify surface and subsurface vortices during the whole year.

e. Complementary tests with χ_T

As mentioned previously, the sea surface density is not currently observed from space and only SST is

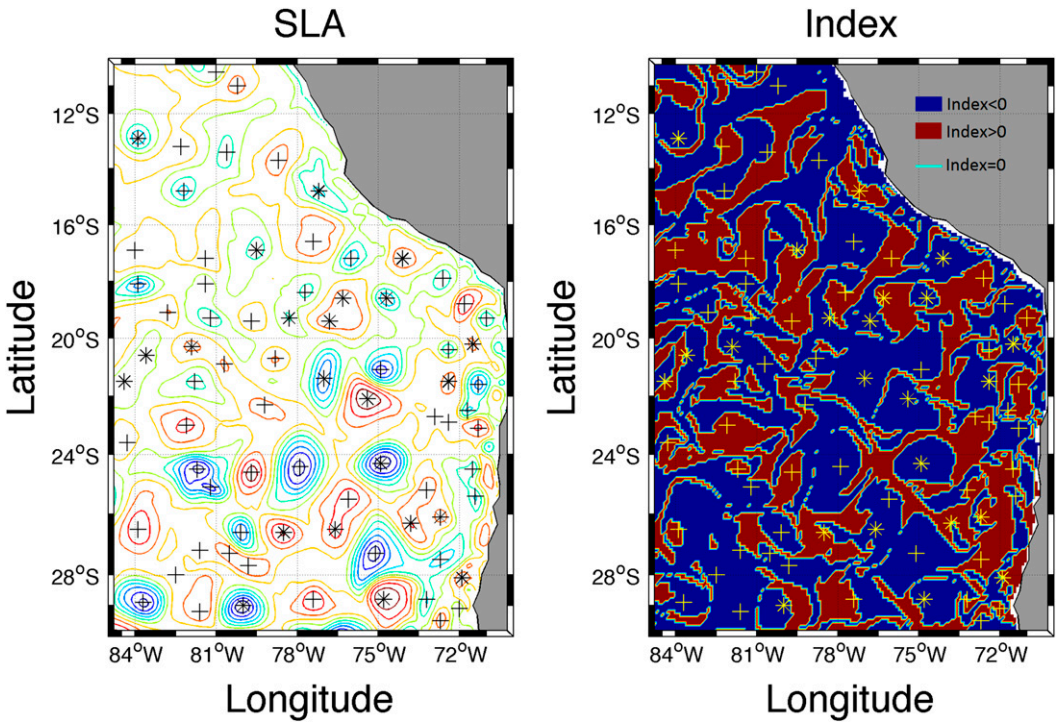

FIG. 9. (left) SLA (as in Fig. 5a, but with fewer contours) and (right) index χ_ρ (as in Fig. 7). Eddies that are correctly identified by the index are labeled with crosses (+). Eddies that are not correctly identified by the index are labeled with stars (*).

available at an adequate resolution and precision. We have thus evaluated the use of χ_T: Fig. 12 is the same as Fig. 9, but using χ_T instead of χ_ρ. The results show a very good general correspondence with χ_ρ. In fact, the nature of eddies, as evaluated from χ_T and χ_ρ, differs from 3% to 8% of the vortices, and most of the eddies with different χ_T and χ_ρ identification are in fact multicore vortices.

Also, the rate of success of using χ_T is 67% for the general case (and 65% for the specific output) below but comparable to the rate associated with χ_ρ. This shows that, in practice, in this region where salinity does not control the stratification, χ_T can be retained without any drastic loss of (qualitative) information in comparison with χ_ρ. Indeed, the differences between the SST and SSS fields are generally due to large-scale variations (characteristics of surface water masses, influence of precipitation, cloud cover, etc.), which is mostly filtered out within the reference state signal. However, regions may exist where vortices are constituted of waters with compensating temperature and salinity anomalies, or regions where the mesoscale signal is dominated by salinity variability, such as close to estuaries. In such cases, the use of χ_T instead of χ_ρ may be more problematic.

7. Conclusions: Summary, discussion, and perspectives

In this work, we have studied the possibility of reconstructing information on the vertical structure of vortices from surface observations. We have first shown that the knowledge of the interior potential vorticity is crucial to determine the exact 3D structure of a vortex in general. Theoretical models based on the pure knowledge of instantaneous surface fields yield good results for surface vortices, but we have shown that subsurface eddies (with an interior potential vorticity field intensified in deep layers) cannot be reconstructed by the SQG or ISQG theories. The ISQG theory improves the results obtained by the SQG theory and can be used for turbulence generated by winds (Rossby waves), where first baroclinic mode and barotropic mode dominate. But, it implicitly hypothesizes that the vortex is surface intensified. ESQG relies on the knowledge of the ocean interior characteristics, which can be calculated from ocean circulation models, but projects SSH on a single vertical profile (which can be surface, subsurface, or mixed) for a given area. The SQG, ISQG, and ESQG approaches thus have to be handled with care in areas where both surface and subsurface vortices exist.

ISQG or ESQG can, however, be extended to take into account other vertical structures, determined from climatologies of specific coherent vortices present in oceanic regions, in particular with subsurface maximum. To do so, a first step is to be able to determine the nature (surface or subsurface) of a vortex from surface fields alone.

We have thus proposed an index to determine the nature (surface or subsurface) of vortices using surface anomalies: the ratio of the sea surface density to the sea level anomalies χ_ρ. This was tested with data coming from a realistic ocean circulation model in the Peru–Chile upwelling system and an analysis of tens of vortices.

We have shown that there exist wrong identifications associated with different error sources. First, in realistic configurations, a filter must be applied to determine the part of the physical fields associated with the vortex signal. We have then shown that the index calculation can be more difficult in a complex environment: a strong current having characteristics similar to the vortex can hide the signal of subsurface eddy when it is located in its vicinity and lead to errors. We have also shown that for multicore structures, with subsurface and surface cores of comparable strength, the determination of the position of the most intense core is difficult, which leads to errors too. This can be problematic in some regions where deep coherent vortices exist but whose signature can be hidden by vertically aligned surface eddies.

The general rate of success of the method reaches 76% in general, multicore vortices representing about half the errors. We have also shown that at first order, the variations of SSρ are dominated by SST variations, except in specific regions, where salinity can play a substantial role on the stratification (near estuaries, region of ice formation/melting, etc.), so that the use of the SST anomaly (a field currently available from satellite observations at high resolution) is a good proxy for the calculation of the index. We think that our results are satisfactory and can be applied to real observations.

A problem to be addressed is then the difference in resolution between satellite SST and SSH data: the spatial and temporal resolutions of infrared SST observations are, for now, far better. This is another potential source of error for the calculation of the index that has to be assessed. In the future, wide-swath altimetric observations will overcome this bias so that the present results will greatly benefit from the breakthrough provided by the Surface Water Ocean Topography (SWOT; http://swot.jpl.nasa.gov/) satellite mission, planned for 2020. Our results are thus also contributions to prepare the exploitation of the future SWOT mission for the analysis of the dynamics of meso- and submesoscale vortices in the ocean. However, for present observations, we expect that applications focusing on large-scale structures or using SST and SSH averaged over several days should limit the problems associated with resolution. Testing the proposed method on different surface and subsurface eddies already identified by authors or using in situ observations is thus an important perspective of this work.

The calculation of the index remains very basic and can certainly be improved. Different attempts have been made to do so. First, we have tried to use a more quantitative approach to identify vortices. Indeed, for surface-intensified vortices, calculations [using Eqs. (4) and (5)] show that the magnitude of SSρ and SLA are linked and should roughly verify

$$H_v \mathrm{SS}\rho/\rho_o \mathrm{SLA} \sim -1, \tag{17}$$

where H_v is the vertical scale of the surface vortex. For subsurface vortices, this ratio should be positive, but weak. We could thus expect that there is a limit of $\chi_\rho < \chi_\rho^{\lim}$ beyond which the vortex is subsurface, instead of a change of sign. This has been applied with success for the main model output analyzed in the paper (associated with Figs. 4–11): using $\chi_\rho^{\lim} = 0.2$ leads to far better results (less than 5% error). However, applying this criterion to the general case was disappointing and even led to degraded general statistics.

We have also thought of replacing SLA with the surface relative vorticity, whose field seems more closely correlated with SSTA (not shown). In the studied region (Southern Hemisphere and negative f), relative vorticity has the same sign as SLA near the vortex center, so that in order to detect surface and subsurface eddies we can use the same algorithms, but we replace SLA by relative vorticity to calculate a new index denoted χ_ρ^ζ.To identify eddies, the same method can be used, but a new minimum ($\zeta_{\min} = 0.5 \times 10^{-5}\,\mathrm{s}^{-1}$) has to be defined to remove weaker eddies. Again the general statistics were not improved in comparison with χ_ρ. In addition, relative vorticity is more difficult to calculate using satellite observations, as gridded altimetric SSH products have a coarse spatial resolution. The relative vorticity field, based on a double derivative of SSH, is then associated with large uncertainties that we believe would be problematic.

Other improvements are possible, such as using an anisotropic filter to better define the anomalies associated with vortices, or trying to better identify the SST anomaly when it is not collocated with the vortex center defined by the SLA extrema. Figure 6 indeed shows that SSρA can be highly variable over the

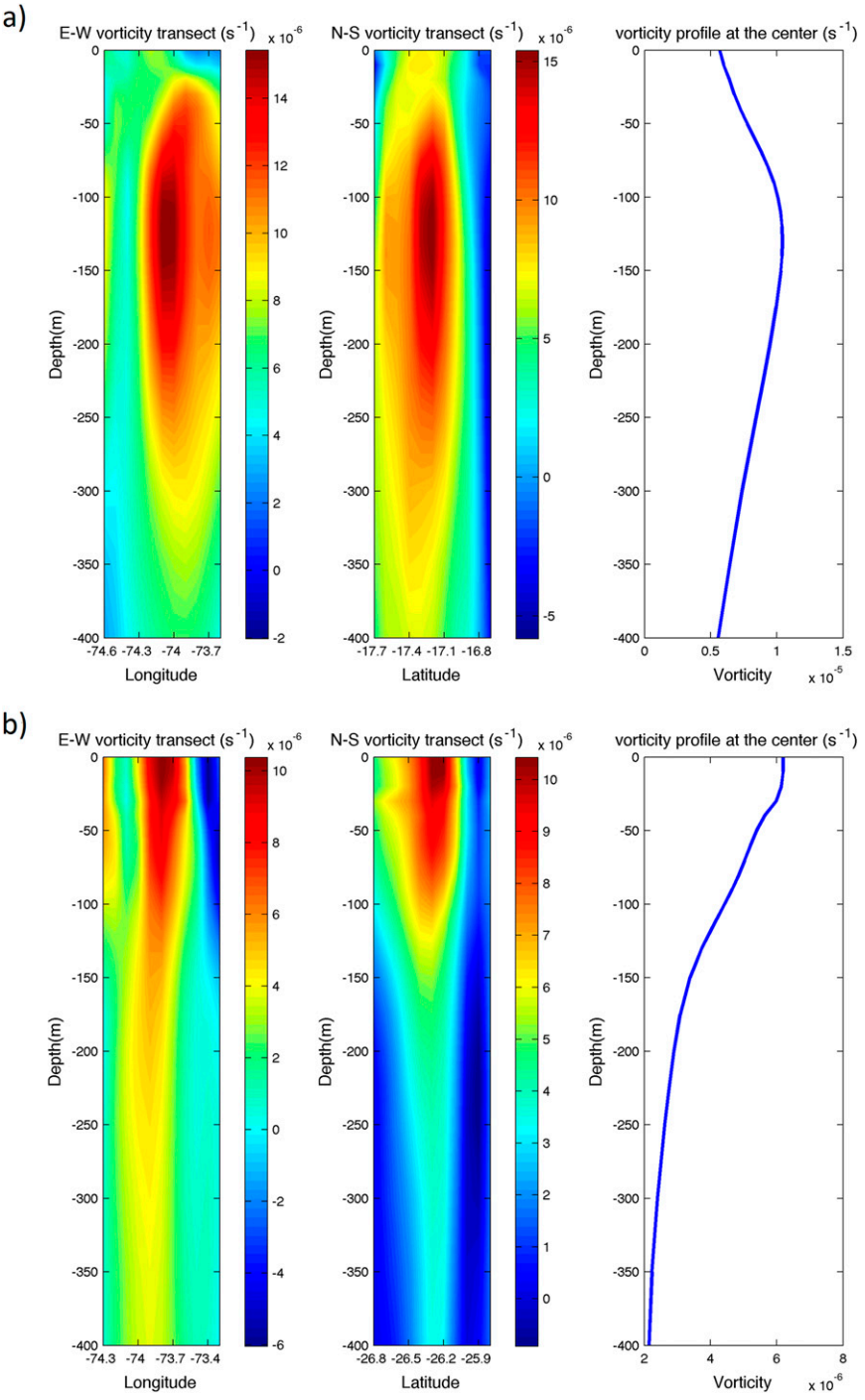

FIG. 10. Vorticity structure of the four eddies for which the index yields wrong results. For each vortex, we have represented the east–west and north–south transects of relative vorticity and a mean vertical profile near the center. The position of each vortex (denoted 10a–d) is given in Fig. 7.

vortex area (delimited by the closed contours of SLA for instance) so that the calculation of the present index can have strong uncertainties given the gap between SLA and SSρ. We believe an index based on an analysis of the latter fields within the vortex area could lead to a significant improvement. However, given its simplicity, we think the present index derived in this first study is useful as a first step.

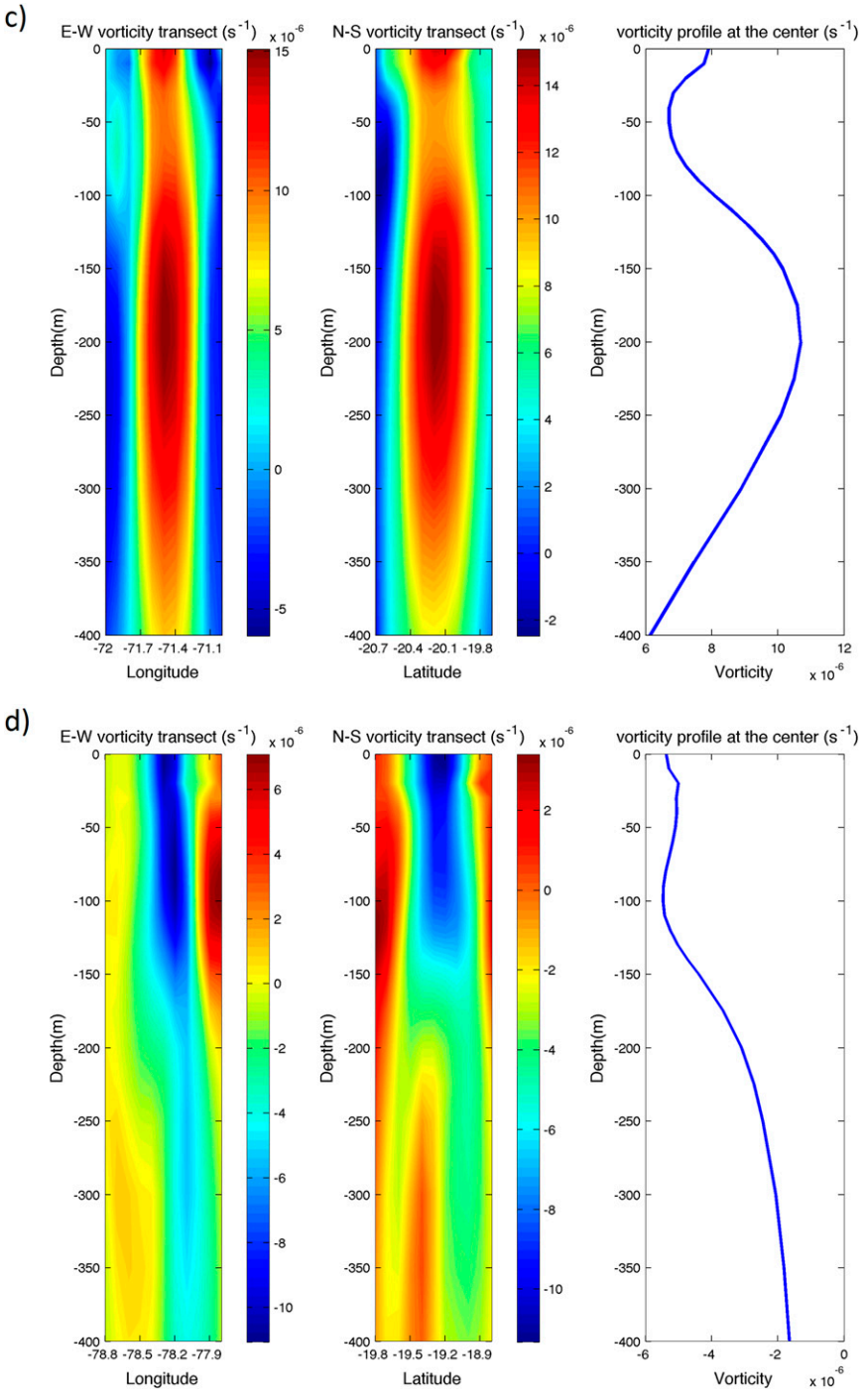

FIG. 10. (*Continued*)

Finally, we have seen here that vortex structures are a complex result of their history. From their formation to their interaction with large-scale background flow, jets or other eddies (such as alignment with other vortices, as mentioned in this paper), or diabatical transformations, many processes can modify their structure. Fundamental studies linking all aspects of vortex evolution to their structure and surface signature are thus of interest also to improve the proposed index or to determine alternative methods for the determination of the nature of vortices.

Concerning applications, we believe the index yields interesting information to determine areas where the

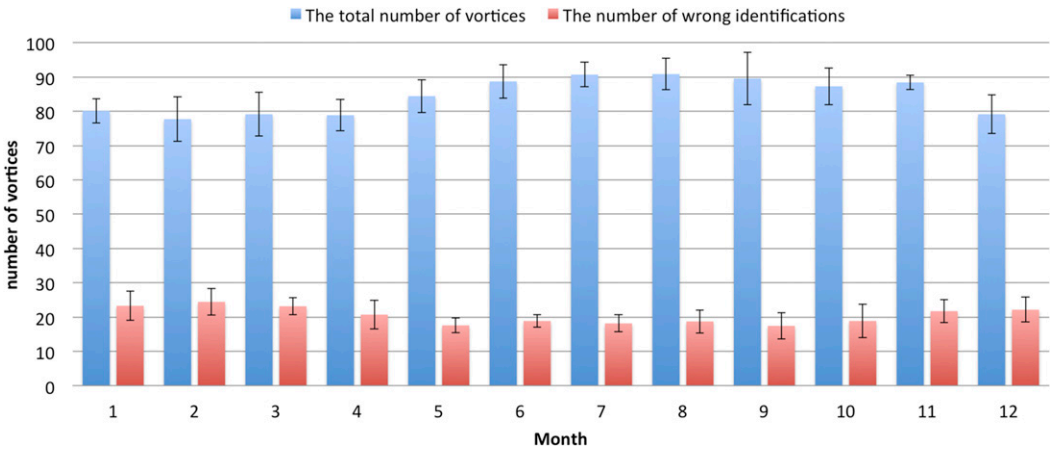

FIG. 11. Diagram representing the monthly statistics of vortices' identification for the numerical simulation used in the study (the black intervals represent the standard deviation for each month over the 7 years of simulation).

SQG approach can be used (or not) to calculate a surface velocity field and where the ISQG method can be generalized to represent subsurface structure, provided the interior PV structure is projected on new vertical profiles, for instance, calculated from local vortex climatologies.

The index can also be applied as a proxy to analyze the details of the processes responsible for the generation and evolution of eddies in nature or in numerical model results, or to evaluate the contribution of eddies to the general circulation in the ocean, in particular in regions where water masses are known to subduct or to surface.

Finally, a straightforward and obvious application of the index is associated with the assimilation of SLA or SST anomalies, which are for now generally associated with surface-intensified eddies. Our work shows that both physical fields are strongly correlated and we think our results offer the first step of a method to combine

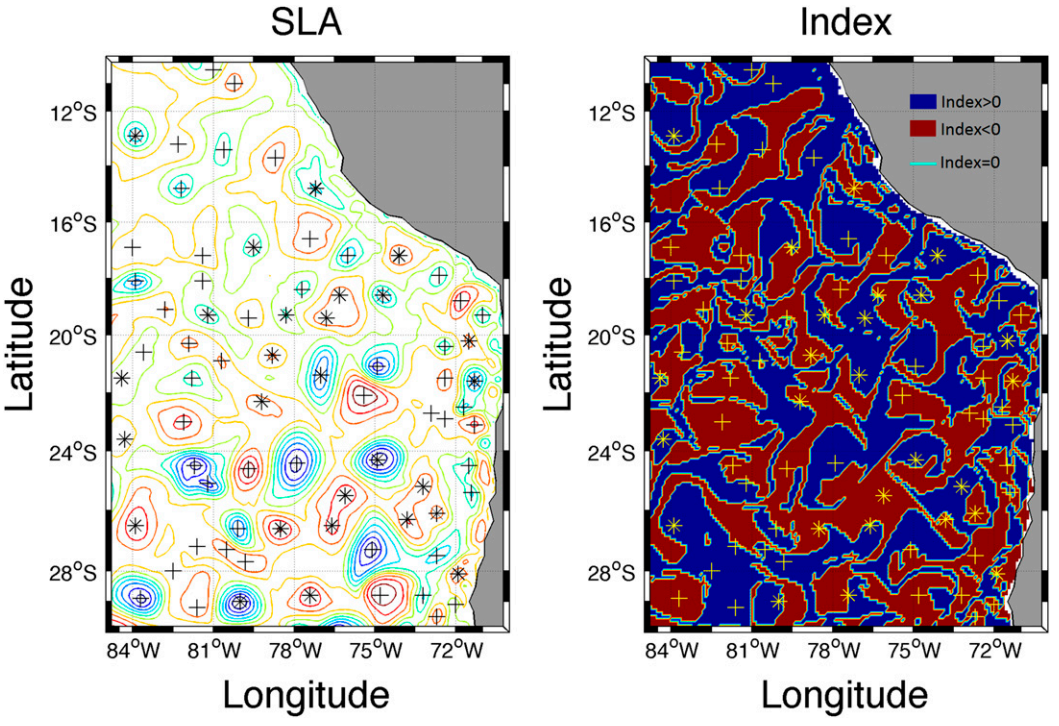

FIG. 12. As in Fig. 9, but using χ_T instead of χ_ρ. Eddies that are correctly identified by the index are labeled with crosses (+). Eddies that are not correctly identified by the index are labeled with stars (*).

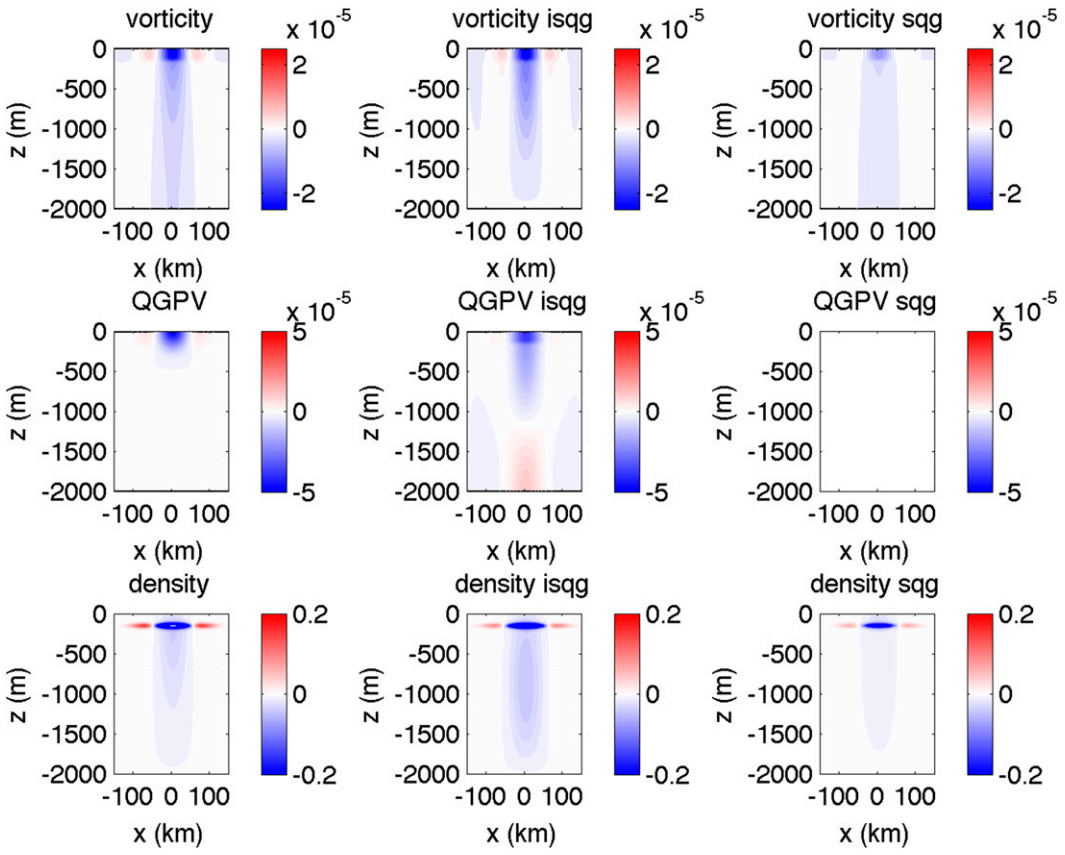

FIG. A1. Vertical section of vorticity, QGPV, and density fields for (left) a surface anticyclone with $\delta\rho_0 = -0.02‰$, $R = 50$ km, $H_v = 200$ m, $z_0 = 0$ m, and $Q_0 = -0.5f$ and reconstructed fields for (center) ISQG and (right) SQG.

them to reconstruct the vertical structure of a vortex and improve the representation of vortices in realistic models with data assimilation. Estimating the exact vertical position of the vortex center remains a problem, as we have shown that the index combines it with the vertical scale of the eddy core and is probably sensitive to the details of the vortex structure. This has to be studied further, but in general a given oceanic region contains a limited number of coherent vortex types. It thus seems possible to determine the index characteristics for each vortex type and to connect an observed anomaly to a single one, then using an average three-dimensional structure of the latter to project the observed anomalies vertically. This, however, requires important further developments.

Acknowledgments. This study has benefited from the funding of different projects: EPIGRAM, funded by CNRS (LEFE/IMAGO) and ANR (Grant ANR-08-BLAN-0330-01); "Merging of satellite and in- situ observations for the analysis of meso and submesoscale dynamics," funded by CNES (OSTST project); and COMODO, funded by Agence Nationale de la Recherche (ANR-11-MONU-005-03). We are grateful to Bernard Le Cann (UBO, LOPS, Brest) for discussions on vortex studies and observations. Dr. Assassi wishes to thank the Space Technology Center (Algeria) for the new position and for letting him finish this work. We are also grateful to the anonymous referees for their comments that drastically improved the quality of the manuscript and the calculation of the index.

APPENDIX A

Evaluation of the SQG and ISQG Methods for Subsurface Vortices

As initially shown by Bretherton (1966), building on the idea that the surface density of the ocean plays the same role as the potential vorticity in the interior of the ocean, several studies have proposed to compute velocity fields from the knowledge of surface temperature alone (see Held et al. 1995; Isern-Fontanet et al. 2006; Lapeyre and Klein 2006), known as the SQG theory (Blumen 1978). It boils down to inverting Eqs. (1), (7), and (8), hypothesizing QGPV = 0. It can be shown that

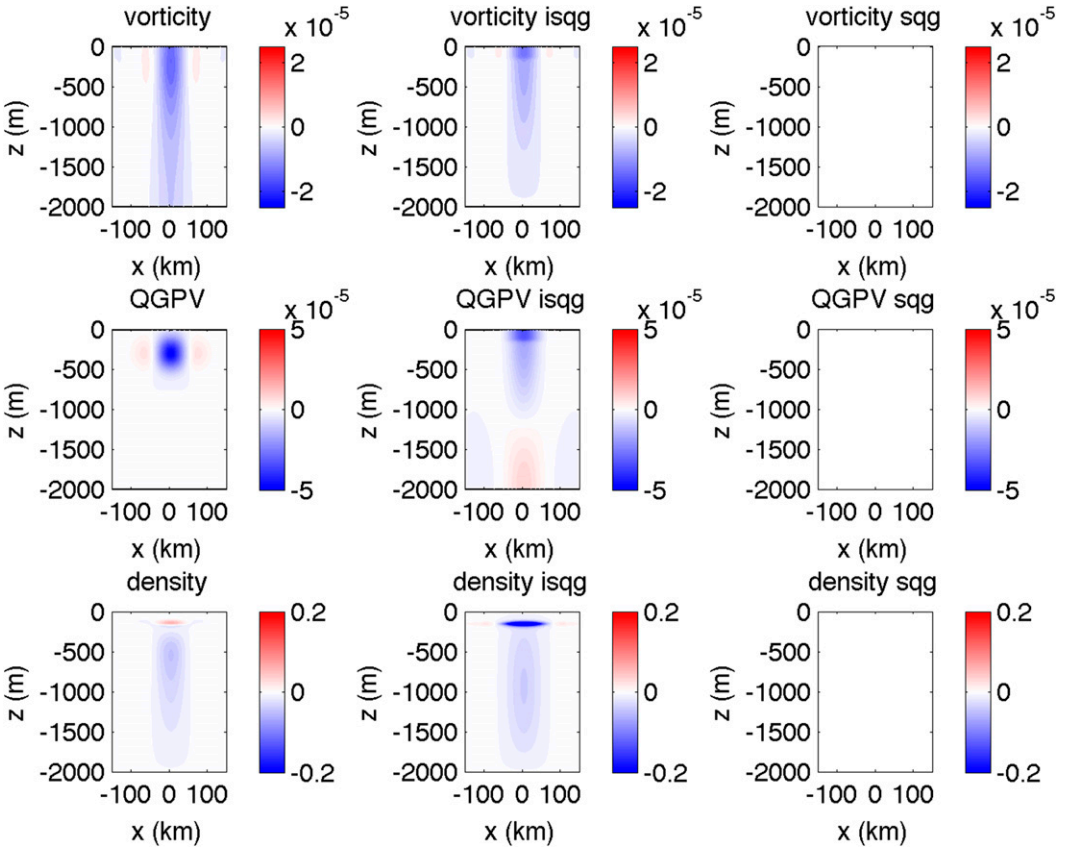

FIG. A2. As in Fig. A1, but for $\delta\rho_0 = 0‰$ and $z_0 = 300$ m.

in the Northern Hemisphere a positive surface density anomaly—or a negative temperature anomaly—will in this case be associated via the SQG theory with a surface-intensified cyclone. Negative surface density anomaly—or a positive temperature anomaly—will be associated by the SQG theory to a surface-intensified anticyclone (see Isern-Fontanet et al. 2006; Lapeyre and Klein 2006).

However, for most oceanic eddies the assumption of no potential vorticity anomaly within the water column is not verified, so we can expect some discrepancies between reconstructed fields using the SQG method and realistic vortex structures. In particular, the difference between the observed sea surface elevation and that obtained using SQG and the sea surface density anomaly is the signature of the interior QGPV.

Based on this idea, Wang et al. (2013) have proposed an improved method, called ISQG, which relies on the addition of an interior streamfunction ψ_i to the SQG streamfunction ψ_{SQG} associated with the surface density anomaly [Eq. (12); $\psi = \psi_{\mathrm{SQG}} + \psi_i$]. The interior streamfunction ψ_i is then calculated, assuming that its vertical structure is a combination of the barotropic and first baroclinic modes whose horizontal structure is calculated so that the total streamfunction matches the sea surface elevation at the surface [$\psi(z = 0) = g\eta/f + \psi_{\mathrm{surf}}$] and vanishes at the bottom. The solution is given by

$$\psi_i(x,y,z) = \psi_h(x,y)F_1(z) - \psi_{\mathrm{SQG}}(x,y,-H) - \psi_h(x,y)F_1(-H), \tag{A1}$$

and

$$\psi_h(x,y) = \frac{1}{F_1(0) - F_1(-H)}[\psi_{\mathrm{surf}}(x,y) + \psi_{\mathrm{SQG}}(x,y,-H) - \psi_{\mathrm{SQG}}(x,y,0)]. \tag{A2}$$

With this, it can be easily verified that $\psi(z = 0) = \psi_{\mathrm{surf}}$ (the sea surface elevation is as prescribed), $\psi(z = -H) = 0$ (the total streamfunction vanishes at the bottom), and $(\partial\psi/\partial z)|_{z=0} = (\partial\psi_{\mathrm{SQG}}/\partial z)|_{z=0}$ (the surface density field is as prescribed). Thus, the ISQG method leads to an estimation of interior fields from the sea surface elevation and density alone and matching these surface fields.

However, the vertical structure of the interior streamfunction, and thus QGPV, is empirically determined and only projects on the barotropic mode (which does not

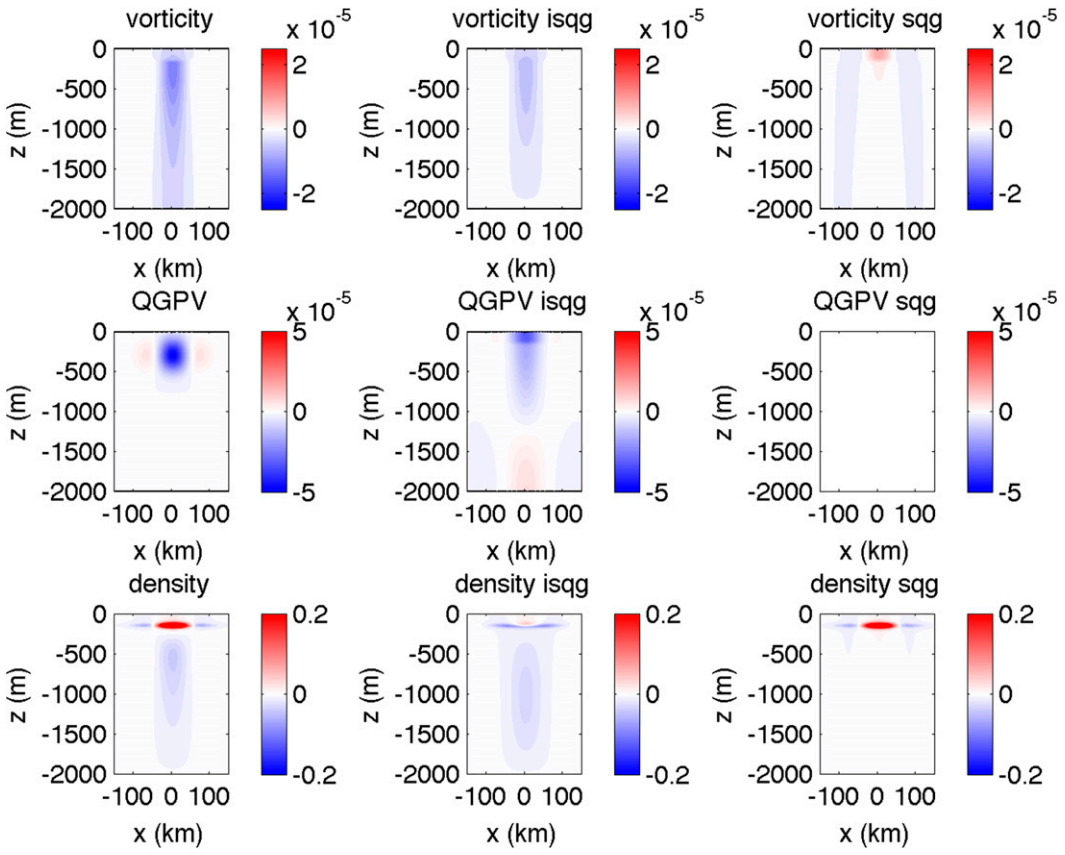

FIG. A3. As in Fig. A2, but for $\delta\rho_0 = 0.02‰$.

vary with depth) and first baroclinic mode. If the details of the shape of the first baroclinic mode depend on the stratification, it is always intensified at the surface, reaches zero at middepth or so and reaches another extreme (usually weaker) at the bottom (see Fig. 1b). As a result, the vertical structure of the QGPV field associated with the ISQG approach is determined by the first baroclinic mode and is always surface intensified.

Figure A1 represents the vorticity, QGPV, and density anomaly fields for a chosen surface-intensified anticyclone with $\delta\rho_0 = -0.02‰$, $R = 50\,\text{km}$, $H_v = 200\,\text{m}$, $z_0 = 0\,\text{m}$, and $Q_0 = -0.5f$ and its reconstruction using the ISQG and SQG approaches. As demonstrated by Wang et al. (2013), the improvement of the ISQG approach is obvious, in particular for the vorticity and density anomaly fields. Notice, however, that there exist discrepancies in the deepest layers for the QGPV field, which exhibits a vertical structure with opposite sign anomalies for ISQG, a structure known to be baroclinically unstable. This modification does not have a strong impact for the reconstructed fields (at least in the upper layers), but if it was used in a predictive model, the evolution and propagation of the (real) QGPV and ISQG reconstructed vortices would be different (see Morel and McWilliams 1997).

As the QGPV of the ISQG is surface intensified (and is null for SQG), the reconstruction of subsurface eddies thus remains a problem for both SQG and ISQG methods. This is illustrated in Fig. A2, which represents the vorticity, QGPV, and density anomaly fields for a subsurface vortex with $\delta\rho_0 = 0‰$, $R = 50\,\text{km}$, $H_v = 200\,\text{m}$, $z_0 = 300\,\text{m}$, and $Q_0 = -0.5f$. The surface vorticity field remains decently represented, but as expected, the QGPV and density fields are this time very different as the structure reconstructed by the ISQG method remains surface intensified. These differences get stronger as the vortex core vertical position (z_0) gets deeper. Also, notice that, as the chosen vortex has no density signature at the surface ($\delta\rho_0 = 0‰$), the SQG fields are null.

Finally, notice that this time the density field reconstructed by the ISQG method leads to opposite-sign anomalies: in fact, an anticyclonic vortex with a negative QGPV core has a weakly stratified core. As a result, surface-intensified anticyclones deflect isopycnic levels and the thermocline downward. This is also true for isopycnic levels located below the core of subsurface vortices, but the isopycnic levels located above their core

are this time pushed upward (see, e.g., Bashmachnikov and Carton 2012; Bashmachnikov et al. 2014).

This has important consequences and accentuates the discrepancies for subsurface anticyclones. Indeed, as isopycnic levels located above the core are pushed upward, it is reasonable to associate this kind of structure with positive density anomalies at the surface. Figure A3 represents the velocity, vorticity, and potential vorticity fields for a subsurface vortex with $\delta\rho_0 = 0.02‰$, $R = 50\,\text{km}$, $H_v = 200\,\text{m}$, $z_0 = 300\,\text{m}$, and $Q_0 = -0.5f$.

The ISQG method leads to subsurface-intensified vorticity, but the QGPV field still has the same problem and the intensity of the vorticity and density fields are this time much weaker than reality. SQG predicts a good thermocline position (density anomaly), but, as a positive surface density anomaly is associated with cyclonic vortices, the vorticity has an opposite sign.

To conclude, both SQG and ISQG have difficulties to represent subsurface eddies. Notice that as Eqs. (1), (7), and (8) are linear, we only considered anticyclonic vortices with a fixed QGPV strength ($Q_0 = -0.5f$), but the results are identical for cyclones or anticyclones with different strength.

The discrepancies associated with the reconstructed ISQG or SQG fields obviously depend on several parameters (vortex core depth, radius, shape, etc.), but subsurface vortices represent a specific problematic category and, despite the recent improvement brought by the ISQG approach, the identification and calculation of the 3D fields for this kind of structures remains a challenge.

APPENDIX B

The Gaussian Filter Algorithm

Using a low-pass filter allows us to retain the large-scale information within an image while reducing the small-scale information. Here, the low-pass filter $\overline{\psi}$ of a physical field ψ is calculated using a smoother of the form:

$$\overline{\psi}(i,j) = \frac{\sum_{\Omega_{i,j}} w(i1,j1)\psi(i1,j1)}{\sum_{\Omega_{i,j}} w(i1,j1)}, \tag{B1}$$

where the weights w are defined as

$$w(i1,j1) = \exp\left\{-\frac{[x(i,j)-x(i1,j1)]^2 + [y(i,j)-y(i1,j1)]^2}{R_f^2}\right\} \tag{B2}$$

and R_f is the correlation radius. The region over which the mean field is calculated is circular with a radius $2R_f$.

REFERENCES

Abraham, E. R., 1998: The generation of plankton patchiness by turbulent stirring. *Nature*, **391**, 577–580, doi:10.1038/35361.

Bashmachnikov, I., and X. Carton, 2012: Surface signature of Mediterranean Water eddies in the north-east Atlantic: Effects of upper layer stratification. *Ocean Sci.*, **8**, 931–943, doi:10.5194/os-8-931-2012.

——, D. Boutov, and J. Dias, 2013: Manifestation of two meddies in altimetry and sea-surface temperature. *Ocean Sci.*, **9**, 249–259, doi:10.5194/os-9-249-2013.

——, X. Carton, and T. V. Belonenko, 2014: Characteristics of surface signature of Mediterranean water eddies. *J. Geophys. Res. Oceans*, **119**, 7245–7266, doi:10.1002/2014JC010244.

Beron-Vera, F. J., M. J. Olascoaga, and G. J. Goni, 2008: Oceanic mesoscale eddies as revealed by Lagrangian coherent structures. *Geophys. Res. Lett.*, **35**, L12603, doi:10.1029/2008GL033957.

——, ——, and ——, 2010: Surface ocean mixing inferred from different multisatellite altimetry measurements. *J. Phys. Oceanogr.*, **40**, 2466–2480, doi:10.1175/2010JPO4458.1.

Bishop, C. H., and A. J. Thorpe, 1994: Potential vorticity and the electrostatics analogy: Quasi-geostrophic theory. *Quart. J. Roy. Meteor. Soc.*, **120**, 713–731, doi:10.1002/qj.49712051710.

Blumen, W., 1978: Uniform potential vorticity flow: Part I. Theory of wave interactions and two-dimensional turbulence. *J. Atmos. Sci.*, **35**, 774–783, doi:10.1175/1520-0469(1978)035<0774:UPVFPI>2.0.CO;2.

Bracco, A., S. Clayton, and C. Pasquero, 2009: Horizontal advection, diffusion, and plankton spectra at the sea surface. *J. Geophys. Res.*, **114**, C02001, doi:10.1029/2007JC004671.

Bretherton, F. P., 1966: Critical layer instability in baroclinic flows. *Quart. J. Roy. Meteor. Soc.*, **92**, 325–334, doi:10.1002/qj.49709239302.

Caballero, A., A. Pascual, G. Dibarboure, and M. Espino, 2008: Sea level and eddy kinetic energy variability in the Bay of Biscay inferred from satellite altimeter data. *J. Mar. Syst.*, **72**, 116–134, doi:10.1016/j.jmarsys.2007.03.011.

Calil, P. H. R., K. J. Richards, Y. Jia, and R. R. Bidigare, 2008: Eddy activity in the lee of the Hawaiian Islands. *Deep-Sea Res. II*, **55**, 1179–1194, doi:10.1016/j.dsr2.2008.01.008.

Carton, J. A., and B. S. Giese, 2008: A reanalysis of ocean climate using Simple Ocean Data Assimilation (SODA). *Mon. Wea. Rev.*, **136**, 2999–3017, doi:10.1175/2007MWR1978.1.

Carton, X., and J. C. McWilliams, 1989: Barotropic and baroclinic instabilities of axisymmetric vortices in a quasigeostrophic model. *Mesoscale/Synoptic Coherent Structures in Geophysical Turbulence*, J. C. J. Nihoul and B. M. Jamart, Eds., Elsevier Oceanography Series, Vol. 50, 225–244, doi:10.1016/S0422-9894(08)70188-0.

Chaigneau, A., and O. Pizarro, 2005a: Surface circulation and fronts of the South Pacific Ocean, east of 120°W. *Geophys. Res. Lett.*, **32**, L08605, doi:10.1029/2004GL022070.

——, and ——, 2005b: Mean surface circulation and mesoscale turbulent flow characteristics in the eastern South Pacific from satellite tracked drifters. *J. Geophys. Res.*, **110**, C05014, doi:10.1029/2004JC002628.

——, A. Gizolme, and C. Grados, 2008: Mesoscale eddies off Peru in altimeter records: Identification algorithms and eddy spatio-temporal patterns. *Prog. Oceanogr.*, **79**, 106–119, doi:10.1016/j.pocean.2008.10.013.

——, G. Eldin, and B. Dewitte, 2009: Eddy activity in the four major upwelling systems from satellite altimetry (1992–2007). *Prog. Oceanogr.*, **83**, 117–123, doi:10.1016/j.pocean.2009.07.012.

——, M. Le Texier, G. Eldin, C. Grados, and O. Pizarro, 2011: Vertical structure of mesoscale eddies in the eastern South Pacific Ocean: A composite analysis from altimetry and Agro profiling floats. *J. Geophys. Res.*, **116**, C11025, doi:10.1029/2011JC007134.

Chelton, D. B., 2013: Ocean–atmosphere coupling: Mesoscale eddy effects. *Nat. Geosci.*, **6**, 594–595, doi:10.1038/ngeo1906.

——, and S. P. Xie, 2010: Coupled ocean-atmosphere interaction at oceanic mesoscales. *Oceanogr. Mag.*, **23**, 52–69, doi:10.5670/oceanog.2010.05.

——, R. A. deSzoeke, M. G. Schlax, K. El Naggar, and N. Siwertz, 1998: Geophysical variability of the first baroclinic Rossby radius of deformation. *J. Phys. Oceanogr.*, **28**, 433–460, doi:10.1175/1520-0485(1998)028<0433:GVOTFB>2.0.CO;2.

——, M. G. Schlax, R. M. Samelson, and R. A. Szoeke, 2007: Global observations of large oceanic eddies. *Geophys. Res. Lett.*, **34**, L15606, doi:10.1029/2007GL030812.

——, ——, and ——, 2011: Global observations of non linear mesoscale eddies. *Prog. Oceanogr.*, **91**, 167–216, doi:10.1016/j.pocean.2011.01.002.

Chérubin, L., X. Carton, J. Paillet, Y. Morel, and A. Serpette, 2000: Instability of the Mediterranean Water undercurrents southwest of Portugal: Effects of baroclinicity and of topography. *Oceanol. Acta*, **23**, 551–573, doi:10.1016/S0399-1784(00)01105-1.

Colas, F., X. Capet, J. C. McWilliams, and A. Shchepetkin, 2008: 1997–1998 El Niño off Peru: A numerical study. *Prog. Oceanogr.*, **79**, 138–155, doi:10.1016/j.pocean.2008.10.015.

——, J. C. McWilliams, X. Capet, and J. Kurian, 2012: Heat balance and eddies in the Peru-Chile current system. *Climate Dyn.*, **39**, 509–529, doi:10.1007/s00382-011-1170-6.

——, X. Capet, J. C. McWilliams, and Z. Li, 2013: Mesoscale eddy buoyancy flux and eddy-induced circulation in eastern boundary currents. *J. Phys. Oceanogr.*, **43**, 1073–1095, doi:10.1175/JPO-D-11-0241.1.

Correard, S., and X. Carton, 1998: Vertical alignment of geostrophic vortices: On the influence of the initial distribution of potential vorticity. *IUTAM Symposium on Simulation and Identification of Organized Structures in Flows*, J. N. Sørensen, E. J. Hopfinger, and N. Aubry, Eds., Fluid Mechanics and Its Applications, Vol. 52, Springer, 191–200, doi:10.1007/978-94-011-4601-2_17.

Cushman-Roisin, B., and J.-M. Beckers, 2011: *Introduction to Geophysical Fluid Dynamics*. 2nd ed. Academic Press, 875 pp.

d'Ovidio, F., V. Fernandez, E. Hernandez-Garcia, and C. Lopez, 2004: Mixing structures in the Mediterranean Sea from finite size Lyapunov exponents. *Geophys. Res. Lett.*, **31**, L17203, doi:10.1029/2004GL020328.

DaSilva, A., A. C. Young, and S. Levitus, 1994: *Algorithms and Procedures*. Vol. 1, *Atlas of Surface Marine Data 1994*, NOAA Atlas NESDIS 6, CD-ROM.

Echevin, V., F. Colas, A. Chaigneau, and P. Penven, 2011: Sensitivity of the Northern Humboldt Current System nearshore modeled circulation to initial and boundary conditions. *J. Geophys. Res.*, **116**, C07002, doi:10.1029/2010JC006684.

Frenger, I., N. Gruber, R. Knutti, and M. Münnich, 2013: Imprint of Southern Ocean eddies on winds clouds and rainfall. *Nat. Geosci.*, **6**, 608–612, doi:10.1038/ngeo1863.

Garfield, N., C. A. Collins, R. G. Paquette, and E. Carter, 1999: Lagrangian exploration of the California Undercurrent. *J. Phys. Oceanogr.*, **29**, 560–583, doi:10.1175/1520-0485(1999)029<0560:LEOTCU>2.0.CO;2.

Held, I. M., R. T. Pierrehumbert, S. T. Garner, and K. L. Swanson, 1995: Surface quasi-geostrophic dynamics. *J. Fluid Mech.*, **282**, 1–20, doi:10.1017/S0022112095000012.

Herbette, S., Y. Morel, and M. Arhan, 2003: Erosion of a surface vortex by a seamount. *J. Phys. Oceanogr.*, **33**, 1664–1679, doi:10.1175/2382.1.

——, ——, and ——, 2004: Subduction of a surface vortex under an outcropping front. *J. Phys. Oceanogr.*, **34**, 1610–1627, doi:10.1175/1520-0485(2004)034<1610:SOASVU>2.0.CO;2.

Hoskins, B. J., M. E. McIntyre, and A. W. Robertson, 1985: On the use and significance of isentropic potential vorticity maps. *Quart. J. Roy. Meteor. Soc.*, **111**, 877–946, doi:10.1002/qj.49711147002.

Isern-Fontanet, J., B. Chapron, G. Lapeyre, and P. Klein, 2006: Potential use of microwave sea surface temperatures for the estimation of ocean currents. *Geophys. Res. Lett.*, **33**, L24608, doi:10.1029/2006GL027801.

Jayne, S. R., and J. Marotzke, 2002: The oceanic eddy heat transport. *J. Phys. Oceanogr.*, **32**, 3328–3345, doi:10.1175/1520-0485(2002)032<3328:TOEHT>2.0.CO;2.

Johnson, G. C., and K. E. McTaggart, 2010: Equatorial Pacific 13°C water eddies in the eastern subtropical South Pacific Ocean. *J. Phys. Oceanogr.*, **40**, 226–236, doi:10.1175/2009JPO4287.1.

Kubryakov, A. A., and S. V. Stanichny, 2015: Seasonal and interannual variability of the Black Sea eddies and its dependence on characteristics of the large-scale circulation. *Deep-Sea Res. I*, **97**, 80–91, doi:10.1016/j.dsr.2014.12.002.

Lapeyre, G., and P. Klein, 2006: Dynamics of the upper oceanic layers in terms of surface quasigeostrophy theory. *J. Phys. Oceanogr.*, **36**, 165–176, doi:10.1175/JPO2840.1.

Lévy, M., and P. Klein, 2004: Does the low frequency variability of mesoscale dynamics explain a part of the phytoplankton and zooplankton spectral variability? *Proc. Roy. Soc. London*, **A460**, 1673–1683, doi:10.1098/rspa.2003.1219.

Marchesiello, P., J. C. McWilliams, and A. Shchepetkin, 2003: Equilibrium structure and dynamics of the California current system. *J. Phys. Oceanogr.*, **33**, 753–783, doi:10.1175/1520-0485(2003)33<753:ESADOT>2.0.CO;2.

Martin, A. P., and K. J. Richards, 2001: Mechanisms for vertical transport within a North Atlantic mesoscale eddy. *Deep-Sea Res. II*, **48**, 757–773, doi:10.1016/S0967-0645(00)00096-5.

McGillicuddy, D. J., 2015: Formation of intrathermocline lenses by eddy–wind interaction. *J. Phys. Oceanogr.*, **45**, 606–612, doi:10.1175/JPO-D-14-0221.1.

——, and A. R. Robinson, 1997: Eddy induced nutrient supply and new production in the Sargasso Sea. *Deep-Sea Res. I*, **44**, 1427–1450, doi:10.1016/S0967-0637(97)00024-1.

——, R. Johnson, D. A. Siege, A. F. Michaels, N. R. Bates, and A. H. Knap, 1999: Mesoscale variations in biogeochemical properties in the Sargasso Sea. *J. Geophys. Res.*, **104**, 13 381–13 394, doi:10.1029/1999JC900021.

McWilliams, J. C., 1985: Submesoscale, coherent vortices in the ocean. *Rev. Geophys.*, **23**, 165–182, doi:10.1029/RG023i002p00165.

——, 1990: The vortices of two-dimensional turbulence. *J. Fluid Mech.*, **219**, 361–385, doi:10.1017/S0022112090002981.

Meunier, T., V. Rossi, Y. Morel, and X. Carton, 2010: Influence of bottom topography on an upwelling current: Generation of long trapped filaments. *Ocean Modell.*, **35**, 277–303, doi:10.1016/j.ocemod.2010.08.004.

Montes, I., F. Colas, X. Capet, and W. Schneider, 2010: On the pathways of the equatorial subsurface currents in the eastern equatorial Pacific and their contributions to the Peru-Chile undercurrent. *J. Geophys. Res.*, **115**, C09003, doi:10.1029/2009JC005710.

——, W. Schneider, F. Colas, B. Blanke, and V. Echevin, 2011: Subsurface connections in the eastern tropical Pacific during La Niña 1999–2001 and El Niño 2002–2003. *J. Geophys. Res.*, **116**, C12022, doi:10.1029/2011JC007624.

Morales, C. E., S. Hormazabel, M. Correa-Ramirez, O. Pizarro, N. Silva, C. Fernandez, V. Anabalon, and M. L. Torreblanco, 2012: Mesoscale variability and nutrient-phytoplankton distribution off central-southern Chile during the upwelling season: The influence of mesoscale eddies. *Prog. Oceanogr.*, **104**, 17–29, doi:10.1016/j.pocean.2012.04.015.

Morel, Y., and J. C. McWilliams, 1997: Evolution of isolated interior vortices in the ocean. *J. Phys. Oceanogr.*, **27**, 727–748, doi:10.1175/1520-0485(1997)027<0727:EOIIVI>2.0.CO;2.

——, and ——, 2001: Effects of isopycnal and diapycnal mixing on the stability of oceanic currents. *J. Phys. Oceanogr.*, **31**, 2280–2296, doi:10.1175/1520-0485(2001)031<2280:EOIADM>2.0.CO;2.

——, D. Darr, and C. Taillandier, 2006: Possible sources driving the potential vorticity structure and long-wave instability of coastal upwelling and downwelling currents. *J. Phys. Oceanogr.*, **36**, 875–896, doi:10.1175/JPO2899.1.

Morrow, R., and P. Y. LeTraon, 2012: Recent advances in observing mesoscale ocean dynamics with satellite altimetry. *Adv. Space Res.*, **50**, 1062–1076, doi:10.1016/j.asr.2011.09.033.

Munk, W. H., and C. Wunsch, 1998: Abyssal recipes II: Energetics of tidal and wind mixing. *Deep-Sea Res. I*, **45**, 1977–2010, doi:10.1016/S0967-0637(98)00070-3.

Nof, D., and W. K. Dewar, 1994: Alignment of lenses: Laboratory and numerical experiments. *Deep-Sea Res. I*, **41**, 1207–1229, doi:10.1016/0967-0637(94)90041-8.

Paillet, J., B. Le Cann, A. Serpette, Y. Morel, and X. Carton, 2002: Dynamics and evolution of a northern meddy. *J. Phys. Oceanogr.*, **32**, 55–79, doi:10.1175/1520-0485(2002)032<0055:DAEOAN>2.0.CO;2.

Pasquero, C., A. Bracco, and A. Provenzale, 2005: Impact of the spatiotemporal variability of the nutrient flux on primary productivity in the ocean. *J. Geophys. Res.*, **110**, C07005, doi:10.1029/2004JC002738.

Pedlosky, J., 1987: *Geophysical Fluid Dynamics*. Springer-Verlag, 710 pp.

Penven, P., V. Echevin, J. Pasapera, F. Colas, and J. Tam, 2005: Average circulation, seasonal cycle, and mesoscale dynamics of the Peru Current System: A modeling approach. *J. Geophys. Res.*, **110**, C10021, doi:10.1029/2005JC002945.

Perrot, X., X. Carton, and A. Guillou, 2010: *Geostrophic vortex alignment in external shear or strain. IUTAM Symposium on Turbulence in the Atmosphere and Oceans*, D. Dritschel, Ed., IUTAM Bookseries, Vol. 28, Springer, 217–224, doi:10.1007/978-94-007-0360-5_18.

Pingree, R. D., and B. Le Cann, 1992a: Three anticyclonic Slope Water Oceanic eDDIES (SWODDIES) in the southern Bay of Biscay in 1990. *Deep-Sea Res.*, **39A**, 1147–1175, doi:10.1016/0198-0149(92)90062-X.

——, and ——, 1992b: Anticyclonic eddy X91 in the southern Bay of Biscay, May 1991 to February 1992. *J. Geophys. Res.*, **97**, 14 353–14 367, doi:10.1029/92JC01181.

——, and ——, 1993: Structure of a meddy (Bobby 92) southeast of the Azores. *Deep-Sea Res. I*, **40**, 2077–2103, doi:10.1016/0967-0637(93)90046-6.

Polvani, L. M., 1991: Two-layer geostrophic vortex dynamics. Part 2. Alignment and two-layer V-states. *J. Fluid Mech.*, **225**, 241–270, doi:10.1017/S0022112091002045.

Ponte, A. L., and P. Klein, 2013: Reconstruction of the upper ocean 3D dynamics from high resolution sea surface height. *Ocean Dyn.*, **63**, 777–791, doi:10.1007/s10236-013-0611-7.

Risien, C. M., and D. B. Chelton, 2008: A global climatology of surface wind and wind stress fields from eight years of QuikSCAT scatterometer data. *J. Phys. Oceanogr.*, **38**, 2379–2413, doi:10.1175/2008JPO3881.1.

Sánchez, R., and J. Gil, 2004: 3D structure, mesoscale interactions and potential vorticity conservation in a swoddy in the Bay of Biscay. *J. Mar. Syst.*, **46**, 47–68, doi:10.1016/j.jmarsys.2003.10.002.

Shchepetkin, A. F., and J. C. McWilliams, 2005: The regional ocean modeling system (ROMS): A split-explicit, free surface, topography following coordinates ocean model. *Ocean Modell.*, **9**, 347–404, doi:10.1016/j.ocemod.2004.08.002.

——, and ——, 2009: Correction and commentary for ''Ocean forecasting in terrain-following coordinates: Formulation and skill assessment of the regional ocean modeling system'' by Haidvogel et al., J. Comp. Phys. 227, pp. 3595–3624. *J. Comput. Phys.*, **228**, 8985–9000, doi:10.1016/j.jcp.2009.09.002.

Stammer, D., H.-H. Hinrichsen, and R. H. Käse, 1991: Can meddies be detected by satellite altimetry? *J. Geophys. Res.*, **96**, 7005–7014, doi:10.1029/90JC02740.

Stramma, L. H., W. Bange, R. Czeschel, A. Lorenzo, and M. Frank, 2013: On the role of mesoscale eddies for the biological productivity and biogeochemistry in the eastern tropical Pacific Ocean off Peru. *Biogeosciences*, **10**, 9179–9211, doi:10.5194/bgd-10-9179-2013.

Sutyrin, G. G., J. C. McWilliams, and R. Saravanan, 1998: Co-rotating stationary states and vertical alignment of geostrophic vortices with thin cores. *J. Fluid Mech.*, **357**, 321–349, doi:10.1017/S0022112097008136.

Sweeney, E. N., D. J. McGillicuddy, and K. O. Buesseler, 2003: Biogeochemical impacts due to mesoscale eddy activity in the Sargasso Sea as measured at the Bermuda Atlantic Time-series. *Deep-Sea Res. II*, **50**, 3017–3039, doi:10.1016/j.dsr2.2003.07.008.

Thompson, A. F., 2008: The atmospheric ocean: eddies and jets in the Antartic Circumpolar Current. *Philos. Trans. Roy. Soc. London*, **A366**, 4529–4541, doi:10.1098/rsta.2008.0196.

Treguier, A. M., J. Deshayes, C. Lique, R. Dussin, and J. M. Molines, 2012: Eddy contributions to the meridional transport of salt in the North Atlantic. *J. Geophys. Res.*, **117**, C05010, doi:10.1029/2012JC007927.

Tychensky, A., and X. Carton, 1998: Hydrological and dynamical characterization of meddies in the Azores region: A paradigm for baroclinic vortex dynamics. *J. Geophys. Res.*, **103**, 25 061–25 079, doi:10.1029/97JC03418.

Vandermeirsch, F., Y. Morel, and G. Sutyrin, 2002: Resistance of a coherent vortex to a vertical shear. *J. Phys. Oceanogr.*, **32**, 3089–3100, doi:10.1175/1520-0485(2002)032<3089:ROACVT>2.0.CO;2.

Wang, J., G. R. Flierl, J. H. LaCasce, J. L. McClean, and A. Mahadevan, 2013: Reconstructing the ocean's interior from surface data. *J. Phys. Oceanogr.*, **43**, 1611–1626, doi:10.1175/JPO-D-12-0204.1.

Wunsch, C., 1999: Where do ocean eddy heat fluxes matter? *J. Geophys. Res.*, **104**, 13 235–13 249, doi:10.1029/1999JC900062.

——, and R. Ferrari, 2004: Vertical mixing, energy, and the general circulation of the oceans. *Annu. Rev. Fluid Mech.*, **36**, 281–314, doi:10.1146/annurev.fluid.36.050802.122121.

Zhang, Z., Y. Zhang, W. Wang, and R. X. Huang, 2013: Universal structure of mesoscale eddies in the ocean. *Geophys. Res. Lett.*, **40**, 3677–3681, doi:10.1002/grl.50736.